exons 2–6, likely the *UGT1A* gene. However, UGT2A3 and each UGT2B are encoded by individual genes. Human UGTs are expressed in a tissue-specific manner.[4] Previous studies using reverse transcription-polymerase chain reaction (PCR) revealed that UGT1A1, UGT1A3, UGT1A4, UGT1A6, UGT1A9, UGT2B4, UGT2B7, UGT2B10, UGT2B11, UGT2B15, and UGT2B17 are expressed in human liver.[4–6]

Mammalian UGTs are located on the endoplasmic reticulum membrane and most of their mass is in the luminal side. That UGTs form homo- or hetero-oligomers was revealed by a variety of techniques including gel permeation chromatography,[7] radiation inactivation analysis,[8,9] a cross-linking study,[10] SDS–PAGE,[11] two-hybrid analysis,[12] a heterologous expression study,[13,14] immobilized metal-chelating chromatography,[15] and fluorescence resonance energy transfer method.[16] Using the heterologous expression technique, we demonstrated that human UGT1A1, UGT1A4, UGT1A6, and UGT1A9 interact with each other via heterodimerization. The heterodimerization of these UGT1A enzymes caused diverse changes of enzyme activities depending on the UGT isoforms and substrates.[17–19] In the present study, we expanded our examination of UGT2B7, because UGT2B7 is the most important isoform for the metabolism of clinically used drugs such as morphine, zidovudine, and valproic acid[20] and is expressed in various tissues including liver, intestine, and kidney. Kurkela et al.[21] has reported that coexpressed UGT1A6 decreased the activity of UGT2B7, but their interaction was not directly proven. Furthermore, there is no information on the interactions between UGT2B7 and the other human UGT1As. In this study, to understand the interactions between UGT2B7 and UGT1A enzymes, we established double expression systems of UGT2B7/UGT1A1, UGT2B7/UGT1A4, UGT2B7/UGT1A6, and UGT2B7/UGT1A9 in HEK293 cells. By native-PAGE analysis, immunoprecipitation assay, and thermal stability assay, we evaluated the significance of the interactions between UGT2B7 and UGT1A enzymes. Finally, the effects of the interactions on their enzyme activities were assessed.

MATERIALS AND METHODS

Chemicals and Reagents

UDPGA, alamethicin, estradiol, and estradiol 3-glucuronide were purchased from Sigma–Aldrich (St. Louis, MO). Zidovudine, imipramine, serotonin, propofol, and G418 were from Wako Pure Chemicals Industries (Osaka, Japan). Zidovudine *O*-glucuronide was obtained from Toronto Research Chemicals (Toronto, Canada). Rabbit anti-human UGT1A polyclonal antibody, rabbit anti-human UGT1A1 polyclonal antibody, rabbit anti-human UGT2B7 polyclonal antibody, and human liver microsomes from 11 individuals were obtained from BD Gentest (Woburn, MA). Rabbit anti-human UGT2B polyclonal antibody (H-300) and goat anti-human UGT2B polyclonal antibody (F-17) were purchased from Santa Cruz Biotechnology (San Diego, CA). Mouse anti-KDEL monoclonal antibody was obtained from Stressgen Biotechnologies (San Diego, CA). Perfect NT Gel M was purchased from DRC (Tokyo, Japan). Primers were commercially synthesized at Hokkaido System Sciences (Sapporo, Japan). All other chemicals and solvents were of analytical grade or the highest grade commercially available.

Stable Single and Double UGT Expression Systems in HEK293 Cells

Expression vectors for human UGT1A1, UGT1A4, UGT1A6, and UGT1A9 were previously constructed.[18] Human UGT2B7 (accession number NM_001074) cDNA was prepared by a reverse transcription-PCR technique from human liver total RNA with sense and antisense oligonucleotide primers (5′-ATT GCA CCA GGA TGT CTG-3′ and 5′-CTT GCA TCA CAA TCT TTC TTG CTG-3′). The PCR products were subcloned into pTARGET Mammalian Expression Vector (Promega, Madison, WI) and the DNA sequences of the inserts were determined using a Thermo Sequenase Cy5.5 Dye Terminator Cycle Sequencing kit (GE Healthcare Bio-Science, Piscataway, NJ) with a Long-Read Tower DNA sequencer (GE Healthcare Bio-Science). HEK293 cells (American Type Culture Collection, Manassas, VA) were grown in Dulbecco's modified Eagle's medium containing 4.5 g/L glucose, 10 mM HEPES, and 10% fetal bovine serum with 5% CO_2 at 37°C. Two micrograms of the UGT expression vector were transfected into HEK293 cells in 6-well plates with Lipofectamine (Invitrogen, Carlsbad, CA). For the double expression systems, the expression vector for UGT2B7 was simultaneously transfected into the cells with each UGT1A expression vector (UGT1A1, UGT1A4, UGT1A6, or UGT1A9) at the ratio of 1:1. Stable transfectants were

selected in medium containing 800 μg/mL G418 and several clones were isolated.

SDS–PAGE or Native-PAGE and Immunoblot Analysis

To determine the expression levels of UGT2B7 and UGT1As in the constructed recombinant systems, SDS–PAGE and immunoblot analysis were performed using anti-UGT2B and anti-UGT1A antibodies and an Odyssey infrared imaging system (Li-COR Biosciences, Lincoln, NE). Since the titer of the rabbit anti-UGT2B antibody was higher than that of the rabbit anti-UGT2B7 antibody, the rabbit anti-UGT2B antibody was used. Although it was confirmed that UGT enzymes are expressed in microsomes fraction, total cell homogenates prepared as described previously[18] were used for convenience in this study. The total cell homogenates (10 μg of protein) were subjected to 10% SDS–PAGE and transferred to a PVDF membrane Immobilon-P (Millipore, Bedford, MA). The membrane was washed with phosphate buffered saline (PBS) two times and blocked with Odyssey Blocking Buffer (Li-COR Biosciences) for 1 h. The membrane was probed with the primary antibody diluted (1:500) with Odyssey Blocking Buffer containing 0.1% Tween-20 for 1 h. The membrane was washed with PBST (PBS containing 0.1% Tween-20) four times and incubated with IRDye680-labeled goat anti-rabbit secondary antibody diluted (1:5000) with PBST for 1 h. The densities of the bands were determined using the Odyssey infrared imaging system. Although the expression levels of UGT2B7 and UGT1As cannot be simply compared because the primary antibodies are different, the relative expression levels of UGT2B7 and UGT1A1 were defined based on standard curves using their single expression systems (1 U/1 mg of cell homogenates) for convenience.

To determine the expression levels of UGT2B7 and UGT1A1 proteins in human liver microsomes, SDS–PAGE and immunoblot analysis were performed using anti-UGT2B7 and anti-UGT1A1 antibodies. For the quantification, the UGT2B7 and UGT1A1 single expression systems were used to make the standard curves as described above.

Native-PAGE analysis was performed to detect monomer and oligomer formations of UGTs as described previously[17] with slight modifications. Ten to 100 μg of total cell homogenates were lysed in solubilizing buffer (0.5% NP-40, 0.25% sodium deoxycholate, 50 mM Tris–HCl (pH 7.5), 150 mM NaCl, and 1 mM EDTA) on ice for 2 h. After centrifugation at 13,000*g* for 30 min, 1 μL of 60% glycerol containing 0.2% bromophenol blue was added to a 20-μL portion of the supernatant. The samples were applied to Perfect NT Gel M (5–20% gradient) and the electrophoresis was carried out at 10 mA for 5 h at 4°C in Tris–glycine electrophoresis buffer (25 mM Tris–base, 192 mM glycine, and 0.1% SDS). The separated proteins were transferred to a PVDF membrane and probed with the anti-UGT2B and anti-UGT1A antibodies as described above.

Immunoprecipitation

Rabbit anti-human UGT1A antibody (BD Gentest) or rabbit anti-human UGT1AC antibody[22] against common carboxyl-terminal region of UGT1A was cross-linked with protein-Sepharose CL-4B (GE Healthcare Bio-Sciences) as described previously.[18] The beads were resuspended in solubilizing buffer (0.5% NP-40, 0.25% deoxycholate, 50 mM Tris–HCl (pH 7.5), 150 mM NaCl, 1 mM EDTA). Cell homogenates (500 μg) were solubilized with the solubilizing buffer in a final concentration of 1.0 mg/mL at 4°C for 2 h. After centrifugation at 13,000*g* for 30 min at 4°C, the supernatants were incubated with the beads at 4°C for 14 h. The beads were washed three times with the solubilizing buffer. The bound proteins were eluted with 2 M guanidine hydrochloride for 6 h at room temperature. The eluates were subjected to SDS–PAGE followed by immunoblot analysis with anti-UGT1A, rabbit or goat anti-UGT2B, and anti-KDEL antibodies.

Glucuronide Formation

Zidovudine *O*-glucuronide formation was determined according to a method by Court et al.[23] with slight modifications. A typical incubation mixture (200 μL total volume) contained 50 mM phosphate buffer (pH 7.4), 5 mM $MgCl_2$, 5 mM UDPGA, 0.2 mg/mL total cell homogenates, alamethicin (50 μg/mg of protein), and 0.25–1.2 mM zidovudine. The reaction was initiated by the addition of UDPGA following a 2 min preincubation at 37°C. The incubation mixture was incubated at 37°C for 60 min, since it was confirmed that the zidovudine *O*-glucuronide formation was linear over 90 min. After the incubation, the reaction was terminated by the addition of 10 μL of 30% perchloric acid.

The reaction mixture was centrifuged at 7,000*g* for 10 min, and 60 μL of the supernatant was subjected to HPLC. The analytical column was an Inertsil ODS-3 (4.6 mm × 250 mm; 5 μm) (GL Sciences, Tokyo, Japan). The mobile phase was 10% acetonitrile/10 mM potassium phosphate buffer (pH 2.3) and the flow rate was 1.0 mL/min. The column eluate was monitored at 267 nm. The retention times of zidovudine *O*-glucuronide and zidovudine were 10.4 and 15.0 min, respectively. The quantification of zidovudine *O*-glucuronide was made by comparing the HPLC peak height to that of the authentic standard.

For the study of thermal stability, reaction mixtures containing the cell homogenate were treated at 47°C for 15 min in the presence of UDPGA. Then, zidovudine was added to the mixture at a final concentration of 250 μM and the mixture was incubated at 37°C for 60 min to determine the residual enzyme activity.

Estradiol 3-*O*-glucuronide formation, imipramine *N*-glucuronide formation, serotonin *O*-glucuronide formation, and propofol *O*-glucuronide formation were determined as described previously.[18]

Kinetic parameters were estimated from the fitted curve using a computer program (KaleidaGraph, Synergy Software, Reading, PA) designed for nonlinear regression analysis. The following equations were used:

Michaelis–Menten equation

$$V = \frac{V_{max}[S]}{K_m + [S]}$$

Hill equation

$$V = \frac{V_{max}[S]^n}{S_{50}^n + [S]^n}$$

Substrate inhibition equation

$$V = \frac{V_{max}[S]}{K_m + [S] + [S]^2/K_i}$$

where V is the velocity of the reaction, S the substrate concentration, K_m the Michaelis–Menten constant, V_{max} the maximum velocity, S_{50} the substrate concentration showing the half V_{max}, n the Hill coefficient, and K_i the substrate inhibition constant. For the Michaelis–Menten kinetics and the substrate inhibition kinetics, the intrinsic clearance (CL_{int}) was calculated as the V_{max}/K_m. For sigmoidal kinetic data, the maximum clearance (CL_{max}), which has been proposed as an appropriate parameter instead of the intrinsic clearance,[24,25] was calculated by the following equation:

$$CL_{max} = \frac{V_{max}}{S_{50}} \frac{(n-1)}{n(n-1)^{1/n}}$$

Statistical Analyses

Data are expressed as mean ± SD of three independent determinations. The statistical significance of the kinetic parameters was determined by analysis of variance (ANOVA) followed by Dunnett's test. A value of $P < 0.05$ was considered statistically significant.

RESULTS

Establishment of Single and Double Expression Systems of UGT2B7 and UGT1As in HEK293 Cells

To investigate whether human UGT2B7 interacts with UGT1A enzymes, stable single expression systems (UGT2B7, UGT1A1, UGT1A4, UGT1A6, and UGT1A9) and double expression systems (UGT2B7/UGT1A1, UGT2B7/UGT1A4, UGT2B7/UGT1A6, and UGT2B7/UGT1A9) in HEK293 cells were constructed. The expression levels of UGT protein were determined by immunoblot analysis (Fig. 1A). The expression levels of UGT2B7 and UGT1A1 in the single expression system were defined as 1.00 U/mg. Based on the expression level of UGT1A1 in the single expression system, the UGT1A4, UGT1A6, and UGT1A9 levels in single expression systems were estimated as 0.18, 0.13, and 0.35 U/mg protein, respectively. In two clones of the double expression system for UGT2B7/UGT1A1, the expression levels of UGT2B7 (0.10 and 0.14 U/mg) and UGT1A1 (0.51 and 0.12 U/mg) resulted in a 2B7/1A ratio 0.2 and 1.2. In two clones of the double expression system for UGT2B7/UGT1A4, the expression levels of UGT2B7 (0.12 and 0.27 U/mg) and UGT1A4 (0.79 and 0.24 U/mg) resulted in a 2B7/1A ratio 0.2 and 1.1. In two clones of the double expression system for UGT2B7/UGT1A6, the expression levels of UGT2B7 (0.22 and 0.12 U/mg) and UGT1A6 (0.57 and 0.09 U/mg) resulted in a 2B7/1A ratio 0.4 and 1.3. In two clones of the double expression system for UGT2B7/UGT1A9, the expression levels of UGT2B7 (0.10 and 0.19 U/mg) and UGT1A9 (0.22 and 0.07 U/mg) resulted in a 2B7/1A ratio 0.5 and 2.7.

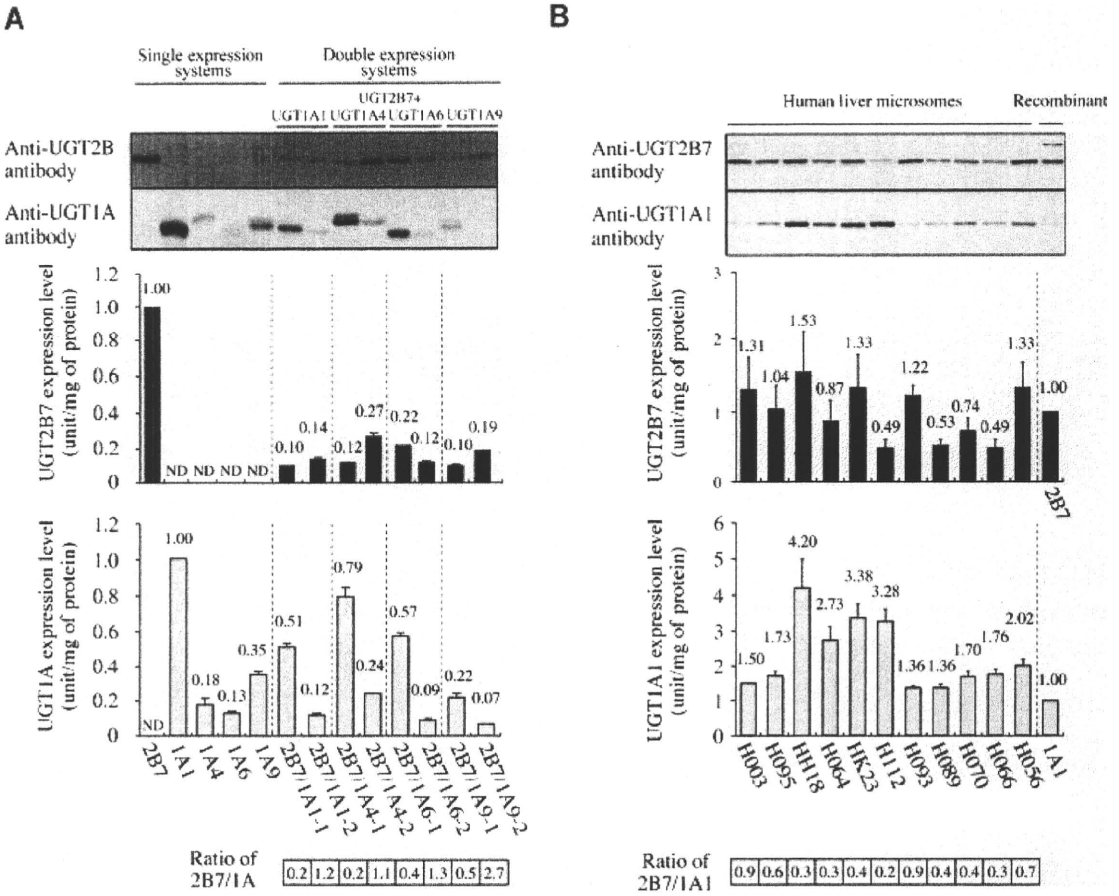

Figure 1. Immunoblot analysis of human UGT2B7 and UGT1As in the single and double expression systems as well as human liver microsomes. The total cell homogenates from the HEK293 expression systems (10 μg protein) were subjected to 10% SDS–PAGE and the membranes were probed with the anti-human UGT2B and anti-human UGT1A antibodies (A). For the analysis of UGT2B7 and UGT1A1 in human liver microsomes, 5- and 2-μg protein of human liver microsomes, respectively, were applied and the membranes were probed with anti-human UGT2B7 and anti-human UGT1A1 antibodies (B). The rightmost lane in the membranes shows the UGT2B7 single expression system (5 μg protein) and the UGT1A1 single expression system (2 μg protein). The expression levels of UGT2B7 and UGT1As were defined based on standard curves using the UGT2B7 and UGT1A1 single expression systems (1 U/1 mg of cell homogenates). Columns are the mean ± SD of three independent determinations.

Expression Levels of UGT1A1 and UGT2B7 Proteins in Human Liver Microsomes

To investigate how similar the UGT2B7/UGT1A ratios in our expression systems were to those in human liver microsomes, we determined the expression levels of UGT2B7 and UGT1A1 protein in human liver microsomes by immunoblot analyses. Since human liver microsomes express multiple UGT isoforms, the specific antibodies against UGT2B7 or UGT1A1 were used. The expression levels were quantified using standard curves of the UGT2B7 and UGT1A1 single expression systems in HEK293 cells. The expression level of UGT2B7 and UGT1A1 proteins in 11 individual human liver microsomes ranged from 0.49 to 1.53 and 1.36 to 4.20 U/mg of protein, respectively (Fig. 1B). The UGT2B7/UGT1A1 ratios ranged from 0.2 to 0.9. These results suggest that the ratios of UGT2B7/UGT1A in our expression systems were similar to the ratios of UGT2B7/UGT1A1 in human liver microsomes.

DOI 10.1002/jps

Native-PAGE Analysis of Single and Double Expression Systems

Native-PAGE analysis was performed to investigate the oligomerizations of human UGT2B7 and UGT1As. First, we confirmed that UGT enzymes were efficiently solubilized with the solubilizing buffer (data not shown). When the total cell homogenate of the single expression system of UGT2B7 was separated, three bands were observed at about 50, 100, and 130 kDa (Fig. 2, arrows 1–3, respectively). These three bands were also observed in the double expression systems of UGT2B7 and UGT1As, but not in Mock cells and the single expression systems of UGT1As. The lower (arrow 1) and middle (arrow 2) bands would correspond to monomers and homodimers, respectively. The upper band (arrow 3) might be an oligomeric form of UGT2B7 that is greater than the dimer. In our previous study,[17] when the double expression system of UGT1A1/UGT1A4 was applied for the native-PAGE analysis, a unique band corresponding to a heterodimer was observed. Interestingly, several bands were detected at around 150–250 kDa in the double expression of UGT2B7 and UGT1As, but not in the single expression system of UGT2B7. Therefore, these unique bands might represent hetero-oligomers of UGT2B7 and UGT1As. To further investigate the hetero-oligomerizations between UGT2B7 and UGT1As, coimmunoprecipitation and thermal stability assay were performed.

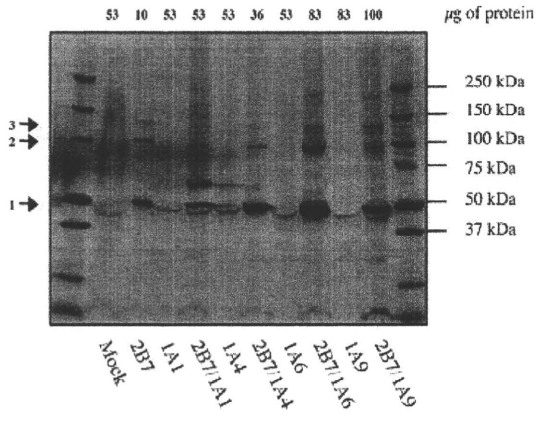

Figure 2. Native-PAGE analyses of UGT2B7 and UGT1As in the single and double expression systems. As the double expression systems, the 2B7/1A1-2, 2B7/1A4-2, 2B7/1A6-2, and 2B7/1A9-2 clones were used. Solubilized total cell homogenates were subjected to gradient gel (5–20%). After electrophoresis at 4°C, the proteins were transferred to a PVDF membrane and immunoblotted with rabbit anti-human UGT2B antibody. Arrows 1–3 represent the bands corresponding to monomer, homodimer, and homo-oligomers of UGT2B7, respectively.

Coimmunoprecipitation of UGT2B7 with Anti-Human UGT1A Antibody

To investigate the association between UGT2B7 and the UGT1A enzymes, immunoprecipitation analysis was carried out using anti-human UGT1A antibody (Fig. 3A). Using the single expression systems, it was confirmed that the anti-human UGT1A antibody specifically immunoprecipitated the UGT1As. When the double expression systems were used, UGT2B7 protein was coimmunoprecipitated by the anti-human UGT1A antibody, although the band density of the UGT2B7 from the double expression system for UGT2B7/1A1 was weaker than those of the other double expression systems. Glucose-regulated protein 94 (GRP94) and GRP78 that are expressed in endoplasmic reticulum were not detected in the immunoprecipitants, indicating the specific interaction between UGT2B7 and the UGT1As. When the anti-human UGT1AC antibody was used for immunoprecipitation, UGT2B7 protein was coimmunoprecipitated from the double expression systems (Fig. 3B). Especially, the band density from the double expression systems for UGT2B7/1A4 and UGT2B7/UGT1A9 was substantial. It was confirmed that UGT1As were immunoprecipitated by the anti-human UGT1AC antibody, and that GRP94 and GRP78 were not detected in the immunoprecipitants. The results suggest that UGT2B7 specifically interacts with the UGT1A enzymes.

Effects of Coexpression of UGT1A on Thermal Instability of UGT2B7

Thermal instability is a useful tool for analyzing protein–protein interactions.[18] As a specific activity for UGT2B7, zidovudine *O*-glucuronidation was measured, since we confirmed that UGT1A1, UGT1A4, UGT1A6, and UGT1A9 could not catalyze this reaction (data not shown). The enzymatic activities in the single and double expression systems were normalized with the UGT2B7 protein levels by immunoblot analysis. Zidovudine *O*-glucuronide formation by the UGT2B7 single expression system was decreased to 5% of control by heat treatment at 47°C for 15 min (Fig. 4), indicating that UGT2B7 is thermally

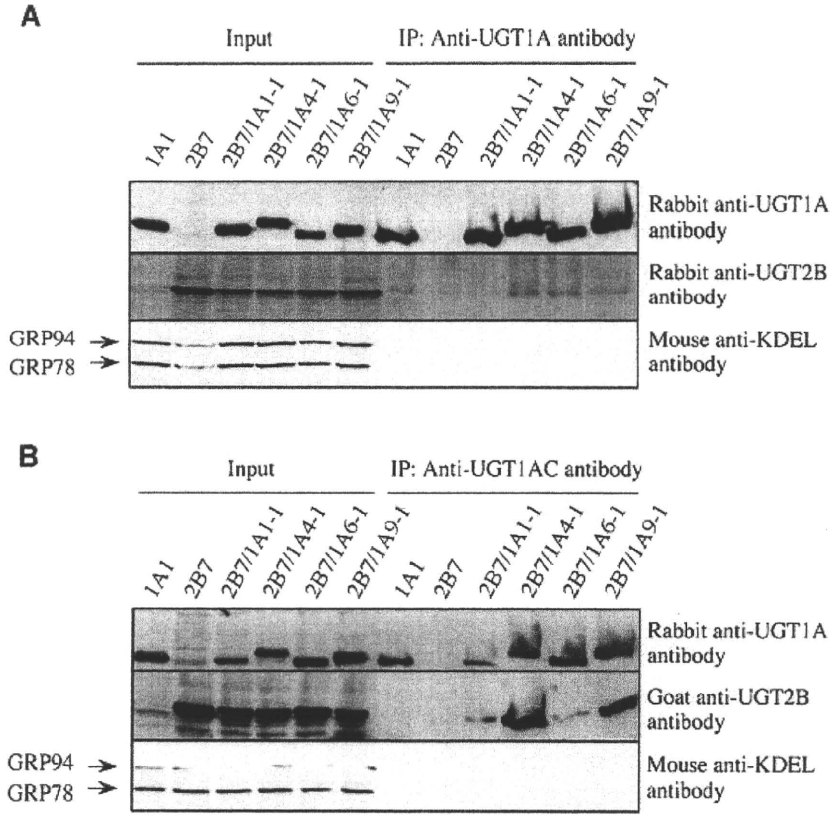

Figure 3. Coimmunoprecipitation of UGT2B7 by anti-human UGT1A antibody using the double expression systems of UGT2B7/UGT1As. Rabbit anti-human UGT1A antibody from BD Gentest (A) or rabbit anti-human UGT1AC antibody prepared by Ikushiro et al.[22] (B) were used for immunoprecipitation. The input proteins and coimmunoprecipitants were subjected to SDS–PAGE followed by immunoblot analysis using anti-human UGT1A, anti-human UGT2B. Anti-KDEL antibodies detected GRP94 and GRP78 only in the input proteins.

instable. UGT2B7 in the double expression systems of UGT2B7/UGT1As showed tolerability to the heat treatment. The results suggest that UGT2B7 interacted with UGT1A1, UGT1A4, UGT1A6, and UGT1A9 in the double expression systems.

Kinetic Analyses of Zidovudine, Estradiol, Imipramine, Serotonin, and Propofol Glucuronide Formations

To investigate the effects of the coexpression of UGT1A enzymes on the enzymatic activity of UGT2B7, kinetic analysis of zidovudine *O*-glucuronide formation was carried out using the single and double expression systems. It was confirmed that any UGT1A enzymes did not show a detectable zidovudine *O*-glucuronide formation (data not shown). The zidovudine *O*-glucuronide formation by the single expression system of UGT2B7 in HEK293 cells fitted to the Michaelis–Menten kinetics (Fig. 5A) with $K_m = 282 \pm 16\ \mu M$, $V_{max} = 449 \pm 16$ pmol/min/U, and $CL_{int} = 1.6 \pm 0.1\ \mu L/min/U$ (Tab. 1). The kinetic parameters were reproducible in another clone of the UGT2B7 single expression system (data not shown). By the coexpression of UGT1A1, the V_{max} and CL_{int} values were significantly increased (Fig. 5A and Tab. 1). By the coexpression of UGT1A4, the K_m value was significantly decreased and the V_{max} and CL_{int} values were significantly increased compared with those values in the UGT2B7 single expression system (Fig. 5B and Tab. 1). A significant decrease of K_m and increases of the V_{max} and CL_{int} values were also observed in the

DOI 10.1002/jps

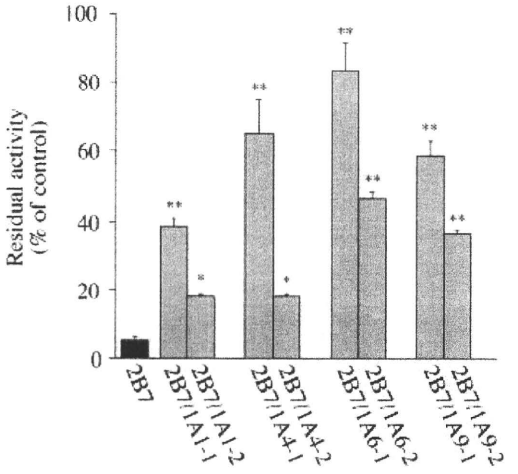

Figure 4. Effect of heat treatment on the enzymatic activities of UGT2B7 in the single and double expression systems. After the preincubation of the total cell homogenates at 47°C for 15 min in the presence of UDPGA, zidovudine *O*-glucuronide formation was measured with 250 μM of substrate. Each column shows the residual activity after the heat treatment. Data are the mean ± SD of three independent determinations. $^{*}P < 0.05$ and $^{**}P < 0.01$ compared with the UGT2B7 single expression system.

double expression systems with UGT1A6 and UGT1A9 (Fig. 5C and D and Tab. 1).

The effects of the coexpression of UGT2B7 on the enzymatic activities of UGT1A1, UGT1A4, UGT1A6, and UGT1A9 were investigated. It was confirmed that the estradiol 3-*O*-glucuronide, imipramine *N*-glucuronide, serotonin *O*-glucuronide, and propofol *O*-glucuronide formations were specifically catalyzed by UGT1A1, UGT1A4, UGT1A6, and UGT1A9, respectively (data not shown). The estradiol 3-*O*-glucuronide formation by the single expression system of UGT1A1 in HEK293 cells followed the Hill equation (Fig. 5E), yielding $S_{50} = 17.5 \pm 3.3$ μM, $V_{max} = 0.8 \pm 0.0$ nmol/min/U, Hill coefficient (n) = 1.4 ± 0.2, and $CL_{max} = 27.0 \pm 2.8$ μL/min/U (Tab. 2). These kinetic parameters were consistent with those of our previous study.[18] By the coexpression of UGT2B7, the S_{50} was significantly decreased and the n value and CL_{max} values were significantly increased (Tab. 2). The imipramine *N*-glucuronide formation by the single expression system of UGT1A4 in HEK293 cells showed substrate inhibition at substrate concentrations >1.5 mM (Fig. 5F). When the kinetics were analyzed by fitting to the Michaelis–Menten kinetics with substrate concentrations up to 1.0 mM, the K_m, V_{max}, and CL_{int} values were 0.6 ± 0.03 mM, 1.4 ± 0.1 nmol/min/U, and 2.3 ± 0.1 μL/min/U, respectively (Tab. 2). By the coexpression of UGT2B7, the K_m and V_{max} values were significantly increased. The serotonin *O*-glucuronide formation by the single expression system of UGT1A6 fitted to the Michaelis–Menten kinetics (Fig. 5G) with $K_m = 7.6 \pm 2.0$ mM, $V_{max} = 2.7 \pm 0.7$ nmol/min/U, and $CL_{int} = 0.4 \pm 0.1$ μL/min/U (Tab. 2). By the coexpression of UGT2B7, the V_{max} and CL_{int} values were increased. The propofol *O*-glucuronide formation by the single expression system of UGT1A9 fitted to the substrate inhibition kinetics (Fig. 5H) with $K_m = 67.7 \pm 5.2$ μM, $V_{max} = 43.7 \pm 3.7$ nmol/min/U, $K_i = 1.0 \pm 0.1$ mM, and $CL_{int} = 0.7 \pm 0.0$ μL/min/U (Tab. 2). The V_{max} and CL_{int} values in the clone 2B7/1A9-1 were significantly increased. These results suggest that UGT2B7 affected the UGT1A1, UGT1A4, UGT1A6, and UGT1A9 activity, and *vice versa*. It was confirmed that mixing of each single expression system did not influence the kinetics of the enzymatic activities (data not shown). Taken together, it is suggested that the coexpressed UGT isoforms functionally interacted with each other in the double expression systems.

DISCUSSION

Accumulating evidence has revealed that UGTs form oligomers.[26] Our previous studies demonstrated that human UGT1A enzymes interact each other via heterodimerization, resulting in changes of the enzymatic properties.[17–19] We expanded out study to investigate whether UGT2B7, one of the major UGT isoforms expressed in human liver, interacts with UGT1As, and to determine the effects of the interaction on the enzymatic activities.

The homo-oligomerizations of human UGT1A enzymes has been demonstrated,[15,16] but it has never been determined whether human UGT2B7 forms homo-oligomers. Previously, we reported that native-PAGE analysis is a useful technique to detect oligomers[17] and we could show the homo-dimerization of UGT1A1, UGT1A4, and UGT1A6. In the present study, the native-PAGE analysis clearly demonstrated the homo-oligomerizations of UGT2B7 (Fig. 2). The results suggested the possibility that UGT2B7 may have the ability to form hetero-oligomer with UGT1A enzymes. Interestingly, bands of hetero-oligomers were also

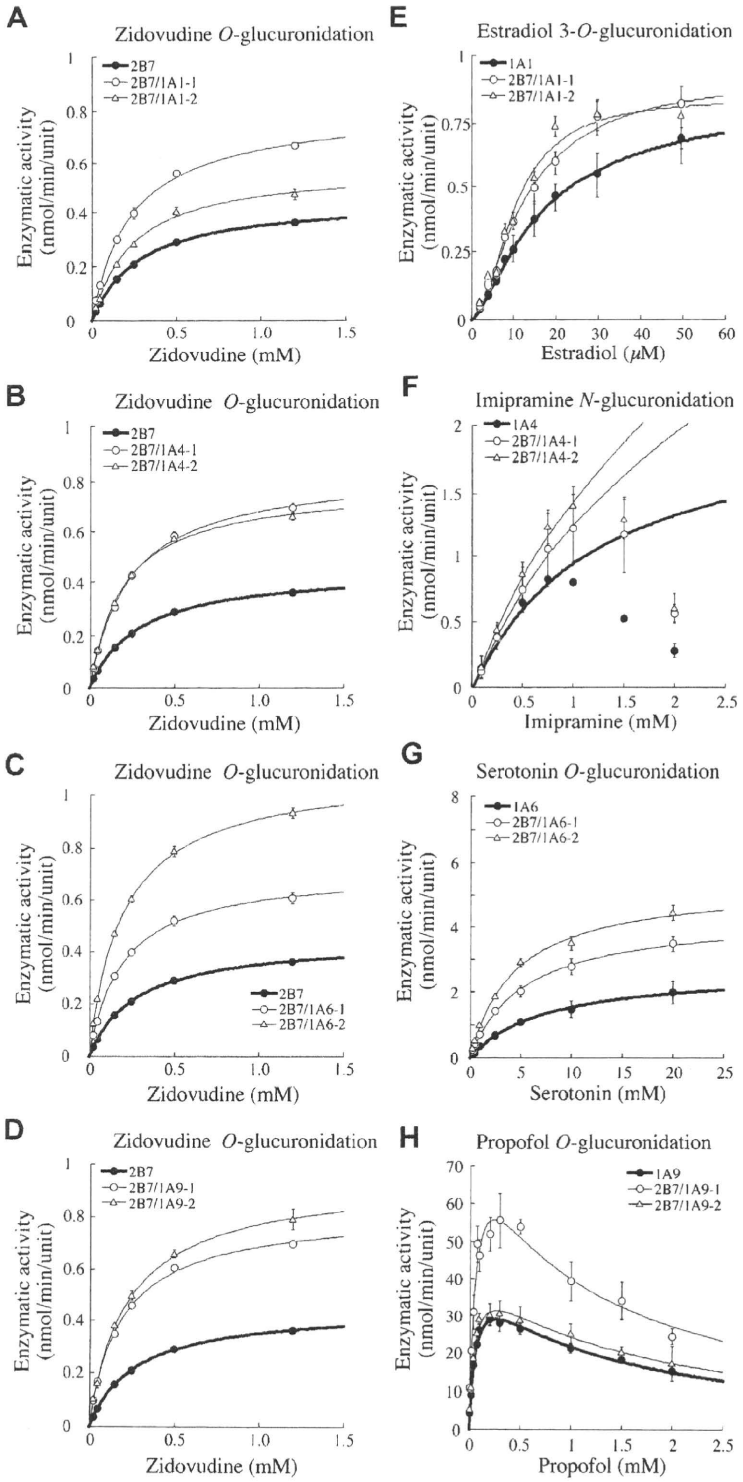

Figure 5. Kinetic analyses of various glucuronide formations by the single and double expression system. Zidovudine *O*-glucuronide formation (A–D), estradiol 3-*O*-glucuronide formation (E), imipramine *N*-glucuronide formation (F), serotonin *O*-glucuronide formation (G), and propofol *O*-glucuronide formation (H) were measured as described in Materials and Methods Section. Data are mean ± SD of three independent determinations.

DOI 10.1002/jps

Table 1. Kinetic Parameters for Zidovudine *O*-Glucuronidation by Single and Double Expression Systems

	K_m (μM)	V_{max} (pmol/min/U)	CL_{int} (μL/min/U)
2B7	282 ± 16	449 ± 16	1.6 ± 0.1
2B7/1A1-1	261 ± 26	824 ± 11**	3.2 ± 0.2**
2B7/1A1-2	261 ± 12	586 ± 23**	2.2 ± 0.0**
2B7/1A4-1	252 ± 14	853 ± 33**	3.4 ± 0.1**
2B7/1A4-2	211 ± 4**	790 ± 16**	3.7 ± 0.1**
2B7/1A6-1	203 ± 3**	719 ± 25**	3.5 ± 0.1**
2B7/1A6-2	197 ± 3**	1090 ± 26**	5.5 ± 0.1**
2B7/1A9-1	196 ± 12**	820 ± 17**	4.2 ± 0.2**
2B7/1A9-2	224 ± 28**	943 ± 58**	4.2 ± 0.3**

Data are mean ± SD of three independent determinations.
**$P < 0.01$ compared with the single expression system.

observed in the double expression systems. The association between UGT2B7 and UGT1A enzymes was proven by immunoprecipitation assay. First, we used the rabbit anti-UGT2B7, rabbit or goat anti-UGT2B antibodies for the immunoprecipitation. However, these antibodies did not successfully immunoprecipitate the UGT2B7 protein (data not shown). Therefore, we used the anti-human UGT1A or anti-human UGT1AC antibodies for immunoprecipitation, which could specifically immunoprecipitate the UGT1A proteins. These antibodies coimmunoprecipitated the UGT2B7 using the double expression systems of UGT2B7/1A, supporting a previous study showing the coimmunoprecipitation of UGT2B7 and UGT1A1 or UGT1A6 using human liver microsomes.[27] When the anti-human UGT1A antibody from BD Gentest was used for immunoprecipitation, coimmunoprecipitated UGT2B7 from the double expression system of UGT2B7/1A1 was lower than those from the other double expression systems (Fig. 3A). When the anti-human UGT1AC antibody prepared by Ikushiro et al.[22] was used for immunoprecipitation, coimmunoprecipitated UGT2B7 from the double expression system of UGT2B7/1A1 and UGT2B7/1A6 was lower than those from the other double expression systems (Fig. 3B). These results may indicate that the extent of interaction with UGT2B7 might vary in

Table 2. Kinetic Parameters for Estradiol 3-*O*-, Imipramine *N*-, Serotonin *O*-, and Propofol *O*-Glucuronidations by Single and Double Expression Systems

	S_{50} (μM)	V_{max} (nmol/min/U)	n	CL_{max} (μL/min/U)
Estradiol 3-*O*-glucuronidation				
1A1	17.5 ± 3.3	0.8 ± 0.0	1.4 ± 0.2	27.0 ± 2.8
2B7/1A1-1	12.6 ± 0.3*	0.9 ± 0.1	1.7 ± 0.1	37.0 ± 2.9**
2B7/1A1-2	9.9 ± 0.5**	0.8 ± 0.1	2.2 ± 0.2**	41.7 ± 1.1**
	K_m (mM)	V_{max} (nmol/min/U)		CL_{int} (μL/min/U)
Imipramine *N*-glucuronidation				
1A4	0.6 ± 0.0	1.4 ± 0.1		2.3 ± 0.1
2B7/1A4-1	2.5 ± 0.3**	4.3 ± 0.8**		1.8 ± 0.5
2B7/1A4-2	2.4 ± 0.4**	4.8 ± 0.2**		2.1 ± 0.3
	K_m (mM)	V_{max} (nmol/min/U)		CL_{int} (μL/min/U)
Serotonin *O*-glucuronidation				
1A6	7.6 ± 2.0	2.7 ± 0.7		0.4 ± 0.1
2B7/1A6-1	5.5 ± 0.7	4.4 ± 0.4*		0.8 ± 0.1**
2B7/1A6-2	4.6 ± 0.8	5.4 ± 0.3**		1.2 ± 0.1**
	K_m (μM)	V_{max} (nmol/min/U)	K_i (mM)	CL_{int} (μL/min/U)
Propofol *O*-glucuronidation				
1A9	67.7 ± 5.2	43.7 ± 3.7	1.0 ± 0.1	0.7 ± 0.0
2B7/1A9-1	64.3 ± 5.4	84.7 ± 7.3**	1.0 ± 0.2	1.3 ± 0.2**
2B7/1A9-2	56.2 ± 6.0	44.4 ± 2.6	1.3 ± 0.2	0.8 ± 0.1

Data are mean ± SD of three independent determinations.
*$P < 0.05$ compared with the single expression system.
**$P < 0.01$ compared with the single expression system.

each UGT1A enzyme. Further validation is needed to estimate the differences in the extent of the hetero-oligomerizations of UGT2B7 and each UGT1A enzyme.

The interaction between UGT2B7 and UGT1A enzymes was supported by the thermal stability study (Fig. 4). UGT2B7 activity was decreased to 5% of control by the heat treatment at 47°C for 15 min in the presence of UDPGA. In contrast, we previously reported that UGT1A1 (60–70% of control), UGT1A4 (80–90% of control), UGT1A6 (90–95% of control), and UGT1A9 (100% of control) could retain their activities after the heat treatment.[18] These results suggest that UGT2B7 is a relatively thermally unstable enzyme. Interestingly, the coexpression of UGT1A enzymes increased the tolerability of UGT2B7. Thus, the findings support the existence of protein–protein interaction between UGT2B7 and UGT1As.

Previously, we reported that human UGT1A1, UGT1A4, UGT1A6, and UGT1A9 interact with each other changing their enzyme kinetics.[17–19] The current study found that UGT2B7 interacts with UGT1A1, UGT1A4, UGT1A6, and UGT1A9 affecting their kinetics and *vice versa* (Fig. 5). Zidovudine *O*-glucuronidation catalyzed by UGT2B7 was increased by the coexpressed UGT1A1, UGT1A4, UGT1A6, and UGT1A9. However, Kurkela et al.[21] has reported that the coexpressed UGT1A6 decreased the zidovudine *O*-glucuronidation and morphine *O*-glucuronidation catalyzed by UGT2B7. The most likely explanation for the discrepancy is that the host cells used were different in our study (HEK293 cells) and their study (Sf9 insect cells). It may be suggested that the differences in the lipid components and/or membrane circumstance may affect the interaction between UGT enzymes. Furthermore, the present study demonstrated that UGT2B7 increased the enzyme activities of UGT1A, UGT1A4, UGT1A6, and UGT1A9 when estradiol, imipramine, serotonin, and propofol were used as substrates. However, we may have to evaluate the activities using multiple substrates, since we previously found that the effects of interaction of UGT1A enzymes were dependent on the substrates.[17] A dose dependency was not observed in the effects on the kinetics between two different clones. We normalized the enzymatic activities with the protein levels determined by SDS–PAGE/immunoblot analysis. However, the detected bands at around 50 kDa would correspond to the sum of monomer and homodimer as well as heterodimer. Thus, the expression ratio of UGT2B/UGT1A may not represent the actual content of heterodimer. This might be one of reasons for no dose dependency.

It is conceivable that all of the human UGT2B and UGT1A enzymes interact in various combinations changing their enzymatic properties. We can envisage that the interaction would occur in human liver microsomes. Usually, recombinant systems express only a single enzyme to evaluate its enzymatic properties. In the case of cytochrome P450, when multiple isoforms are involved in a given metabolic pathway, the data obtained from the recombinant enzymes can be applied to predict the contribution of each cytochrome P450 enzyme, because the activity of a certain P450 isoform is not affected by other isoforms and because we can determine the absolute expression levels of each P450 protein in human liver microsomes. This theory could not be applied for UGT because of their complicated interactions depending on the UGT isoforms, substrates, and the expression ratios of multiple UGT isoforms, even if we can determine the absolute protein expression levels of each UGT enzyme. Thus, it would be difficult to fully understand the contribution of each UGT isoform from the output activity in human liver microsomes.

In conclusion, the present study demonstrated that UGT2B7 protein interacts with UGT1A1, UGT1A4, UGT1A6, and UGT1A9 proteins. The interactions affected their enzymatic activities and resulted in altered kinetic parameters for glucuronidations. Such complicated interactions would also make difficult the prediction of *in vivo* clearance from *in vitro* data.

ACKNOWLEDGMENTS

We acknowledge Brent Bell for reviewing the manuscript.

REFERENCES

1. Dutton GJ. Acceptor substrates of UDP glucuronosyltransferase and their assay. In: Dutton GJ, editor. Glucuronidation of drugs and other compounds. Boca Raton, FL: CRC Press. 1980. pp. 69–78.
2. Mackenzie PI, Walter Bock K, Burchell B, Guillemette C, Ikushiro S, Iyanagi T, Miners JO, Owens IS, Nebert DW. 2005. Nomenclature update for the mammalian UDP glycosyltransferase (UGT) gene

superfamily. Pharmacogenet Genomics 15:677–685.
3. Ritter JK, Chen F, Sheen YY, Tran HM, Kimura S, Yeatman MT, Owens IS. 1992. A novel complex locus UGT1 encodes human bilirubin, phenol, and other UDP-glucuronosyltransferase isozymes with identical carboxyl termini. J Biol Chem 267:3257–3261.
4. Tukey RH, Strassburg CP. 2000. Human UDP-glucuronosyltransferases: Metabolism, expression and disease. Annu Rev Pharmacol Toxicol 40:581–616.
5. Fisher MB, Paine MF, Strelevitz TJ, Wrighton SA. 2001. The role of hepatic and extrahepatic UDP-glucuronosyltransferases in human drug metabolism. Drug Metab Rev 33:273–297.
6. Nakamura A, Nakajima M, Yamanaka H, Fujiwara R, Yokoi T. 2008. Expression of UGT1A and UGT2B mRNA in human normal tissues and various cell lines. Drug Metab Dispos 36:1461–1464.
7. Matern H, Matern S, Gerok W. 1982. Isolation and characterization of rat liver microsomal UDP-glucuronosyltransferase activity toward chenodeoxycholic acid and testosterone as a single form of enzyme. J Biol Chem 257:7422–7429.
8. Peters WH, Jansen PL, Nauta H. 1984. The molecular weights of UDP-glucuronosyltransferase determined with radiation-inactivation analysis. a molecular model of bilirubin UDP-glucuronyltransferase. J Biol Chem 259:11701–11705.
9. Gschaidmeier H, Bock KW. 1994. Radiation inactivation analysis of microsomal UDP-glucuronosyltransferases catalysing mono- and diglucuronide formation of 3,6-dihydroxybenzo(a)pyrene and 3,6-dihydroxychrysene. Biochem Pharmacol 48: 1545–1549.
10. Ikushiro S, Emi Y, Iyanagi T. 1997. Protein-protein interactions between UDP-glucuronosyltransferase isozymes in rat hepatic microsomes. Biochemistry 36:7154–7161.
11. Meech R, Mackenzie PI. 1997. UDP-glucuronosyltransferase, the role of the amino terminus in dimerization. J Biol Chem 272:26913–26917.
12. Ghosh SS, Sappal BS, Kalpana GV, Lee SW, Chowdhury JR, Chowdhury NR. 2001. Homodimerization of human bilirubin-uridine-diphosphoglucuronate glucuronosyltransferase-1 (UGT1A1) and its functional implications. J Biol Chem 276:42108–42115.
13. Ishii Y, Miyoshi A, Watanabe R, Tsuruda K, Tsuda M, Yamaguchi-Nagamatsu Y, Yoshisue K, Tanaka M, Maji D, Ohgiya S, Oguri K. 2001. Simultaneous expression of guinea pig UDP-glucuronosyltransferase 2B21 and 2B22 in COS-7 cells enhances UDP-glucuronosyltransferase 2B21-catalyzed morphine-6-glucuronide formation. Mol Pharmacol 60: 1040–1048.
14. Kurkela M, Hirvonen J, Kostiainen R, Finel M. 2004. The interactions between the N-terminal and C-terminal domains of the human UDP-glucuronosyltransferases are partly isoform-specific and may involve both monomers. Biochem Pharmacol 68:2443–2450.
15. Kurkela M, Garcia-Horsman JA, Luukkanen L, Morsky S, Taskinen J, Baumann M, Kostiainen R, Hirvonen J, Finel M. 2003. Expression and characterization of recombinant human UDP-glucuronosyltransferases (UGTs). UGT1A9 is more resistant to detergent inhibition than the other UGTs and was purified as an active dimeric enzyme. J Biol Chem 278:3536–3544.
16. Operana TN, Tukey RH. 2007. Oligomerization of the UDP-glucuronosyltransferase 1A proteins. Homo- and heterodimerization analysis by fluorescence resonance energy transfer (FRET) and co-immunoprecipitation. J Biol Chem 282:4821–4829.
17. Fujiwara R, Nakajima M, Yamanaka H, Katoh M, Yokoi T. 2007. Interactions between human UGT1A1, UGT1A4, and UGT1A6 affect their enzymatic activities. Drug Metab Dispos 35:1781–1787.
18. Fujiwara R, Nakajima M, Yamanaka H, Nakamura A, Katoh M, Ikushiro S, Sakaki T, Yokoi T. 2007. Effects of coexpression of UGT1A9 on enzymatic activities of human UGT1A isoforms. Drug Metab Dispos 35:747–757.
19. Nakajima M, Yamanaka H, Fujiwara R, Katoh M, Yokoi T. 2007. Stereoselective glucuronidation of 5-(4′-hydroxyphenyl)-5-phenylhydantoin by human UDP-glucuronosyltransferase (UGT) 1A1, UGT1A9, and UGT2 B15: Effects of UGT-UGT interactions. Drug Metab Dispos 35:1679–1686.
20. Williams JA, Hyland R, Jones BC, Smith DA, Hurst S, Goosen TC, Peterkin V, Koup JR, Ball SE. 2004. Drug-drug interactions for UDP-glucuronosyltransferase substrates: A pharmacokinetic explanation for typically observed low exposure (AUCi/AUC) ratios. Drug Metab Dispos 32:1201–1208.
21. Kurkela M, Patana AS, Mackenzie PI, Court MH, Tate CG, Hirvonen J, Goldman A, Finel M. 2007. Interactions with other human UDP-glucuronosyltransferases attenuate the consequences of the Y485D mutation on the activity and substrate affinity of UGT1A6. Pharmacogenet Genomics 17:115–126.
22. Ikushiro S, Emi Y, Kato Y, Yamada S, Sakaki T. 2006. Monospecific antipeptide antibodies against human hepatic UDP-glucuronosyltransferase 1A subfamily (UGT1A) isoforms. Drug Metab Pharmacokinet 21:70–74.
23. Court MH, Krishnaswamy S, Hao Q, Duan SX, Patten CJ, Von Moltke LL, Greenblatt DJ. 2003. Evaluation of 3′-azido-3′-deoxythymidine, morphine, and codeine as probe substrates for UDP-glucuronosyltransferase 2B7 (UGT2B7) in human liver microsomes: Specificity and influence of the UGT2B7*2 polymorphism. Drug Metab Dispos 31: 1125–1133.

24. Houston JB, Kenworthy KE. 2000. In vitro-in vivo scaling of CYP kinetic data not consistent with the classical Michaelis-Menten model. Drug Metab Dispos 28:246–254.
25. Uchaipichat V, Mackenzie PI, Guo XH, Gardner-Stephen D, Galetin A, Houston JB, Miners JO. 2004. Human UDP-glucuronosyltransferases, isoform selectivity and kinetics of 4-methylumbelliferone and 1-naphthol glucuronidation, effects of organic solvents, and inhibition by diclofenac and probenecid. Drug Metab Dispos 32:413–423.
26. Finel M, Kurkela M. 2008. The UDP-glucuronosyltransferases as oligomeric enzymes. Curr Drug Metab 9:70–76.
27. Fremont JJ, Wang RW, King CD. 2005. Coimmunoprecipitation of UDP-glucuronosyltransferase isoforms and cytochrome P450 3A4. Mol Pharmacol 67:260–262.

DOI 10.1002/jps

THE JOURNAL OF BIOLOGICAL CHEMISTRY VOL. 285, NO. 7, pp. 4415–4422, February 12, 2010

MicroRNAs Regulate Human Hepatocyte Nuclear Factor 4α, Modulating the Expression of Metabolic Enzymes and Cell Cycle*

Received for publication, November 16, 2009, and in revised form, December 12, 2009 Published, JBC Papers in Press, December 15, 2009, DOI 10.1074/jbc.M109.085431

Shingo Takagi[1], **Miki Nakajima, Katsuhiko Kida, Yu Yamaura, Tatsuki Fukami, and Tsuyoshi Yokoi**[2]

From Drug Metabolism and Toxicology, Division of Pharmaceutical Sciences, Graduate School of Medical Science, Kanazawa University, Kakuma-machi, Kanazawa 920-1192, Japan

Hepatocyte nuclear factor (HNF) 4α is a key transcription factor regulating endo/xenobiotic-metabolizing enzymes and transporters. We investigated whether microRNAs are involved in the regulation of human HNF4α. Potential recognition elements for miR-24 (MRE24) were identified in the coding region and the 3′-untranslated region (3′-UTR), and those for miR-34a (MRE34a) were identified in the 3′-UTR in HNF4α mRNA. The HNF4α protein level in HepG2 cells was markedly decreased by the overexpression of miR-24 and miR-34a. The HNF4α mRNA level was significantly decreased by the overexpression of miR-24 but not by miR-34a. In luciferase analyses in HEK293 cells, the reporter activity of plasmid containing the 3′-UTR of HNF4α was significantly decreased by miR-34a. The reporter activity of plasmid containing the HNF4α coding region downstream of the *luciferase* gene was significantly decreased by miR-24. These results suggest that the MRE24 in the coding region and MRE34a in the 3′-UTR are functional in the negative regulation by mRNA degradation and translational repression, respectively. The down-regulation of HNF4α by these microRNAs resulted in the decrease of various target genes such as cytochrome P450 7A1 and 8B1 as well as morphological changes and the decrease of the S phase population in HepG2 cells. We also clarified that the expressions of miR-24 and miR-34a were regulated by protein kinase C/mitogen-activated protein kinase and reactive oxygen species pathways, respectively. In conclusion, we found that human HNF4α was down-regulated by miR-24 and miR-34a, the expression of which are regulated by cellular stress, affecting the metabolism and cellular biology.

Human hepatocyte nuclear factor 4α (HNF4α, NR2A1),[3] which belongs to the nuclear hormone receptor superfamily, is highly expressed in liver and regulates the expression of various genes involved in the synthesis/metabolism of fatty acid, cholesterol, glucose, and urea (1). It is well recognized that endo/xenobiotic-metabolizing enzymes such as cytochrome P450s (CYPs), UDP-glucuronosyltransferases, sulfotransferase as well as ATP-binding cassette transporters, organic anion transporters and organic cation transporters are under the control of HNF4α (2). HNF4α transactivates the expression of target genes not only via direct binding to their regulatory sequences but also through the regulation of other transcriptional factors such as pregnane X receptor and constitutive androstane receptor, which regulate these target genes. HNF4α forms large transcriptional regulatory networks in the liver. Therefore, it is believed that the change of HNF4α expression has a great impact upon the function of the liver.

Bile acids are important regulatory molecules mediating cholesterol synthesis and glucose metabolism as well as their own synthesis (3). It is well known that HNF4α positively regulates the expression of bile acid-synthesizing enzymes such as CYP7A1 and CYP8B1. When bile acids are accumulated, the HNF4α-mediated transactivation is inhibited by short heterodimer partner, which is up-regulated by bile acid-activating farnesoid X receptor (4, 5). Bile acids are known to activate the mitogen-activated protein kinase (MAPK) signaling pathway. It is known that the expression and function of HNF4α are up- or down-regulated through extracellular signal-regulated kinase (ERK), c-Jun NH_2-terminal kinase (JNK), and p38 MAPK pathways (6–8). In addition, chenodeoxycholic acid, a toxic bile acid, has been reported to decrease the HNF4α mRNA expression via unknown pathways (9). Thus, the bile acid synthesis would be fine-tuned through the modulation of the expression and/or activity of HNF4α. However, the regulatory mechanism of the HNF4α expression has not still been fully understood.

MicroRNAs (miRNAs) are a recently discovered family of short noncoding RNA whose final product is an ~22-nucleotide functional RNA molecule (10). They regulate the expression of target genes by binding to complementary regions of transcripts to repress their translation or mRNA degradation. At present, more than 700 miRNAs have been identified in humans. They are expressed in a cell- or tissue-specific manner. For example, miR-122 is most abundantly and specifically expressed in liver (11). It has been demonstrated that silencing

* This work was supported in part by a grant-in-aid for scientific research (B) from the Japan Society for the Promotion of Science and in part by a Health and Labor Science Research Grant from the Ministry of Health, Labor and Welfare of Japan.

[1] Research Fellow of the Japan Society for the Promotion of Science.

[2] To whom correspondence should be addressed: Drug Metabolism and Toxicology, Faculty of Pharmaceutical Sciences, Kanazawa University, Kakuma-machi, Kanazawa 920-1192, Japan. Tel./Fax: 81-76-234-4407; E-mail: tyokoi@kenroku.kanazawa-u.ac.jp.

[3] The abbreviations used are: HNF, hepatocyte nuclear factor; RT, reverse transcription; UTR, untranslated region; miRNA, microRNA; CYP, cytochrome P450; MAPK, mitogen-activated protein kinase; ERK, extracellular signal-regulated kinase; JNK, c-Jun NH_2-terminal kinase; PMA, phorbol 12-myristate 13-acetate; GAPDH, glyceraldehyde-3-phosphate dehydrogenase; HA, hemagglutinin; siRNA, small interfering RNA; PEPCK, phosphoenolpyruvate carboxykinase; pre-miR, precursor miR; GFP, green fluorescent protein; FACS, fluorescence-activated cell sorter; PKC, protein kinase C; ROS, reactive oxygen species.

TABLE 1
Primers for real time RT-PCR
The nucleotide sequences of miRNAs and the others were adopted from miRBase sequences and the GenBank™ database, respectively.

Target gene	Accession No.	Forward (5′ to 3′)	Reverse (5′ to 3′)
HNF4α	NM_000457	TGTCCCGACAGATCACCTC	CACTCAACGAGAACCAGCAG
CYP7A1	NM_000780	CAGTGCCTCCCTCAACATCC	GACATATTGTAGCTCCCGATCC
CYP8B1	NM_004391	CTACACGAAGGACAAGGAGCAGGAC	GTGGCTCACGGAGAGCATCTTGTG
CYP27A1	NM_000784	GGCAACGGAGCTTAGAGGAGATTC	CATCCACATTGGACCGTACTTGGC
PEPCK	NM_002591	AGCTCGGTCGCTGGATGTCAGAG	GTAGGGTGAATCCGTCAGCTCGATG
p16	NM_000077	TGCCCAACGCACCGAATAGTTACG	TGCACGGGTCGGGTGAGAG
p21	NM_000389	CTGTCACTGTCTTGTACCCTTGTGC	GGAGAAGATCAGCCGGCGTTTG
p27	NM_004064	AGCAATGCGCAGGAATAAGGAAGCG	GTTTGACGTCTTCTGAGGCCAGG
GAPDH	NM_002046	CCAGGGCTGCTTTTAACTC	GCTCCCCCCTGCAAATGA
U6 snRNA	NR_004394	CGCTTCGGCAGCACATATACTAA	TATGGAACGCTTCACGAATTTGC
Pre-miR-24-1	MI0000080	TCCGGTGCCTACTGAGCTGATATC	CTGTTCCTGCTGAACTGAGCCA
Pre-miR-24-2	MI0000081	CGTGCCTACTGAGCTGAAACACAG	CTGTTCCTGCTGAACTGAGCCA
Pre-miR-34a	MI0000268	CCAGCTGTGAGTGTTTCTTTGGCAG	CCCACAACGTGCAGCACTTCTAG
miR-24	MIMAT0000080	TGGCTCAGTTCAGCAGGAACAG	Universal qPCR primer
miR-34a	MIMAT0000255	TGGCAGTGTCTTAGCTGGTTGT	Universal qPCR primer

of miR-122 *in vivo* causes a decrease of hepatic cholesterol biosynthesis (12). In addition, two independent studies revealed that the knockdown of all miRNAs in liver by conditional knock-out of Dicer1 resulted in apoptosis and inflammation (13) or a disruption of hepatic zonation (14). These findings indicate the physiological and biological significance of miRNAs in liver function. In this study, we examined the possibility that miRNAs might regulate the expression of human HNF4α, resulting in the modulation of liver function.

EXPERIMENTAL PROCEDURES

Chemicals and Reagents—Phorbol 12-myristate 13-acetate (PMA), H_2O_2, U0126, and SB202190 were obtained from Wako Pure Chemicals (Osaka, Japan). SP600125 was from Calbiochem. The pGL3-promoter (pGL3p) vector, pGL4.74-TK plasmid, pTARGET vector, and dual luciferase reporter assay system were purchased from Promega (Madison, WI). Lipofectamine 2000, Lipofectamine RNAiMAX, Stealth Select RNA interference for human HNF4α (HSS140902) (siHNF4α), and Negative Control Medium GC Duplex #3 (siControl) were from Invitrogen. Pre-miR miRNA precursor molecule for miR-24, miR-34a, and Negative Control #1 (Control) were from Ambion (Austin, TX). All of the primers were commercially synthesized at Hokkaido System Sciences (Sapporo, Japan). Goat anti-human HNF4α polyclonal antibodies (S-20), rabbit anti-human GAPDH polyclonal antibodies, and mouse anti-HA monoclonal antibodies were from Santa Cruz Biotechnology (Santa Cruz, CA), IMGENEX (San Diego, CA), and COVANCE (Berkeley, CA), respectively. Alexa Fluor 680 donkey anti-goat IgG was from Invitrogen. IRDye 680 goat anti-rabbit IgG and goat anti-mouse IgG were from LI-COR Biosciences (Lincoln, NE). All other chemicals and solvents were of the highest grade commercially available.

Cell Culture—The human hepatocellular carcinoma cell line HepG2 was obtained from Riken Gene Bank (Tsukuba, Japan). The human embryonic kidney cell line HEK293 was obtained from American Type Culture Collection (Manassas, VA). HepG2 cells were cultured in Dulbecco's modified Eagle's medium (Nissui Pharmaceutical, Tokyo, Japan) supplemented with 0.1 mM nonessential amino acid (Invitrogen) and 10% fetal bovine serum (Invitrogen). HEK293 cells were cultured in Dulbecco's modified Eagle's medium supplemented with 4.5 g/liter glucose, 10 mM HEPES, and 10% fetal bovine serum. These cells were maintained at 37 °C under an atmosphere of 5% CO_2, 95% air.

Transfection of miRNAs or siRNA into HepG2 Cells—Pre-miR miRNA precursor molecule and siRNA were transfected into HepG2 cells using Lipofectamine RNAiMAX. Unless otherwise specified, the pre-miR miRNA Precursor Molecule and siRNA were transfected at final concentrations of 50 and 5 nM, respectively. After 48 h, total RNA was isolated using RNAiso according to the manufacturer's protocol. Whole cell lysates were prepared by homogenization with lysis buffer (50 mM Tris-HCl, pH 8.0, 150 mM NaCl, 1 mM EDTA, 1% Nonidet P-40) containing protease inhibitors (0.5 mM (*p*-amidinophenyl)-methanesulfonyl fluoride, 2 μg/ml aprotinin, 2 μg/ml leupeptin, 2 μg/ml pepstatin). The protein concentrations were determined using Bradford protein assay reagent (Bio-Rad) with γ-globulin as a standard.

Real Time RT-PCR for HNF4α, Its Target Genes, and miRNAs—The cDNAs were synthesized from total RNA using ReverTra Ace (Toyobo, Osaka, Japan). The primers used are shown in Table 1. The real time PCR was performed using the Mx3000P (Stratagene, La Jolla, CA) with the MxPro QPCR software as follows: after an initial denaturation at 95 °C for 2 min, the amplification was performed by denaturation at 95 °C for 15 s, annealing, and extension at 65 °C for 20 s for 40 cycles. The mRNA levels of HNF4α, phosphoenolpyruvate carboxykinase (PEPCK), p16, p21, p27, and CYPs were normalized with the GAPDH mRNA level, and the levels of pre-miR-24-1, pre-miR-24-2, pre-miR-34a, and mature miRNAs were normalized with the U6 small nuclear RNA level. For the quantification of mature miRNAs, reverse transcription was performed using the NCode miRNA first strand cDNA synthesis kit (Invitrogen) according to the manufacturer's protocol.

SDS-PAGE and Western Blot Analyses—The whole cell lysates (20 μg) were separated with 10% SDS-polyacrylamide gel electrophoresis and transferred to Immobilon-P transfer membrane (Millipore, Bedford, MA). The membranes were probed with goat anti-human HNF4α, rabbit anti-human GAPDH, or mouse anti-HA antibodies and the corresponding fluorescent dye-conjugated second antibodies. The band densities were quantified with an Odyssey infrared imaging system (LI-COR Biosciences). The HNF4α protein level was evaluated as the sum of the densities of two bands.

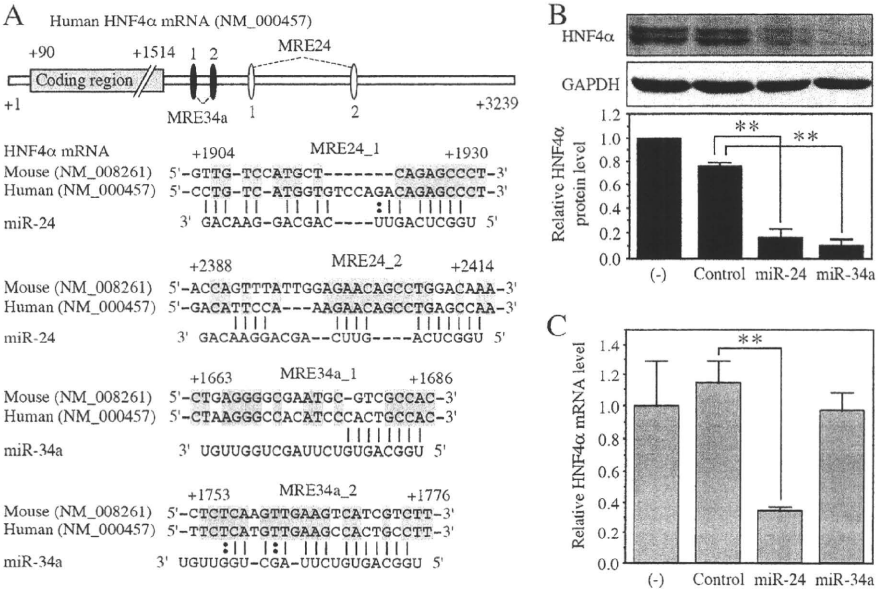

FIGURE 1. **The potential MREs in the 3′-UTR of HNF4α mRNA and the effects of miR-24 and miR-34a on the HNF4α level.** *A*, schematic diagrams of human HNF4α mRNA and the predicted target sites of miR-24 and miR-34a in the 3′-UTR are shown (*upper panel*). The numbering refers to the 5′ end of mRNA as 1. Complementarity of miR-24 and miR-34a to the predicted target sequence of human HNF4α is shown (*lower panel*). The conserved nucleotides are highlighted in *gray boxes*. *B* and *C*, pre-miR miRNA precursor molecules were transfected into HepG2 cells at a concentration of 50 nM. After 48 h, total RNA and whole cell lysates were prepared. The HNF4α and GAPDH protein levels were determined by Western blot analyses (*B*). The HNF4α mRNA levels were determined by real time RT-PCR and normalized with the GAPDH mRNA level (*C*). The data are relative to no transfection (−). Each column represents the mean ± S.D. of three independent experiments. **, $p < 0.01$.

Construction of Plasmids—Human HNF4α cDNA including coding region and 3′-untranslated region (UTR) was amplified by PCR using cDNA prepared from HepG2 with the forward primer 5′-agaatgcgactctccaaaaccctc-3′ and the reverse primer 5′-tgaattctccttaatatttatcagcaaac-3′. From this fragment, the HNF4α coding region was digested with PmaCI. These cDNA fragments were cloned into the pTARGET vector (Promega), resulting in pTARGET/HNF4α+3′-UTR and pTARGET/HNF4α plasmids. HA-tagged GFP expression plasmid was constructed by PCR using pGSU6-GFP plasmid (Genlantis, San Diego, CA) as a template with the forward primer, 5′-tttacgcgtatgtacccctacgacgtgcccgactacgccatggctagcaaaggagaagaac-3′ (HA tag is underlined), and the reverse primer, 5′-tttgcggccgctcagttgtacagttcatccatgc-3′. To construct luciferase reporter plasmids, various fragments of the HNF4α coding region or 3′-UTR were inserted into the XbaI site downstream of the *luciferase* gene in the pGL3p vector. The nucleotide sequences of the constructed plasmids were confirmed by DNA sequencing analyses.

Transient Expression of HNF4α in HEK293 Cells and Transfection of miRNAs—The pTARGET/HNF4α and pTARGET/HNF4α+3′-UTR plasmids were transiently transfected with HA-tagged GFP expression plasmid and pre-miR miRNA precursor molecules into HEK293 cells. Briefly, the day before transfection, the cells were seeded into 24-well plates. After 24 h, 450 ng of the HNF4α expression plasmid, 50 ng of the pTARGET/HA-tagged GFP plasmid, and 50 nM of pre-miR miRNA precursor molecules were transfected using Lipofectamine 2000. After incubation for 48 h, the cells were harvested, and whole cell lysates were prepared as described above.

Luciferase Assay—Various luciferase reporter plasmids (pGL3p) were transiently transfected with pGL4.74-TK plasmid into HEK293 cells. Briefly, the day before transfection, the cells were seeded into 24-well plates. After 24 h, 90 ng of pGL3p plasmid, 10 ng of pGL4.74-TK plasmid, and 10 nM of pre-miR miRNA precursor molecules were transfected into HEK293 cells using Lipofectamine 2000. After incubation for 48 h, the cells were resuspended in the passive lysis buffer, and then the luciferase activity was measured with a luminometer (Wallac, Turku, Finland) using a dual luciferase reporter assay system.

Treatment of HepG2 Cells with Chemicals—HepG2 cells were seeded into 12-well plates, and after 24 h, the cells were treated with 100 nM PMA or 500 μM H_2O_2 for the indicated times. The specific inhibitors for MAPK, U0126, SB202190, and SP600125 were co-treated with PMA for 1 h or with H_2O_2 for 6 h at a final concentration of 10 μM. Total RNA was isolated as described above.

Cell Cycle Analysis—HepG2 cells were fixed with 70% ethanol at 48 h after the transfection of pre-miR miRNA precursor molecules or siRNAs. The cells were washed with FACS buffer (phosphate-buffered saline containing 0.1% bovine serum albumin) and incubated with FACS buffer containing 50 μg/ml RNase A for 30 min at 37 °C. The cells were stained with 25 μg/ml propidium iodide and analyzed using FACSCalibur and Cell Quest Pro software (BD Biosciences, San Jose, CA). Synchronization of HepG2 cells were carried out by serum deprivation. After 24 h, the cells were restimulated with serum for the indicated time.

Statistical Analysis—Statistical significance was determined by analysis of variance followed by Dunnett multiple comparisons test or Tukey method test. A value of $p < 0.05$ was considered statistically significant.

RESULTS

miR-24 and miR-34a Down-regulate HNF4α—The length of the 3′-UTR of human HNF4α is ~1.7 kb (Fig. 1*A*). Computational prediction using miRanda, PicTar, and TargetScan identified the potential recognition elements for various miRNAs including miR-1, miR-24, miR-34a, miR-326, and miR-485 in the 3′-UTR of HNF4α. Among them, we decided to investigate the effects of miR-24 and miR-34a on HNF4α expression, because they were predicted by two algorithms. Western blot analysis using whole cell lysates from HepG2 cells showed two bands of HNF4α, probably corresponding to variants 1 and 2 (Fig. 1*B*). Variant 2 is a natural splicing variant with 30 nucleo-

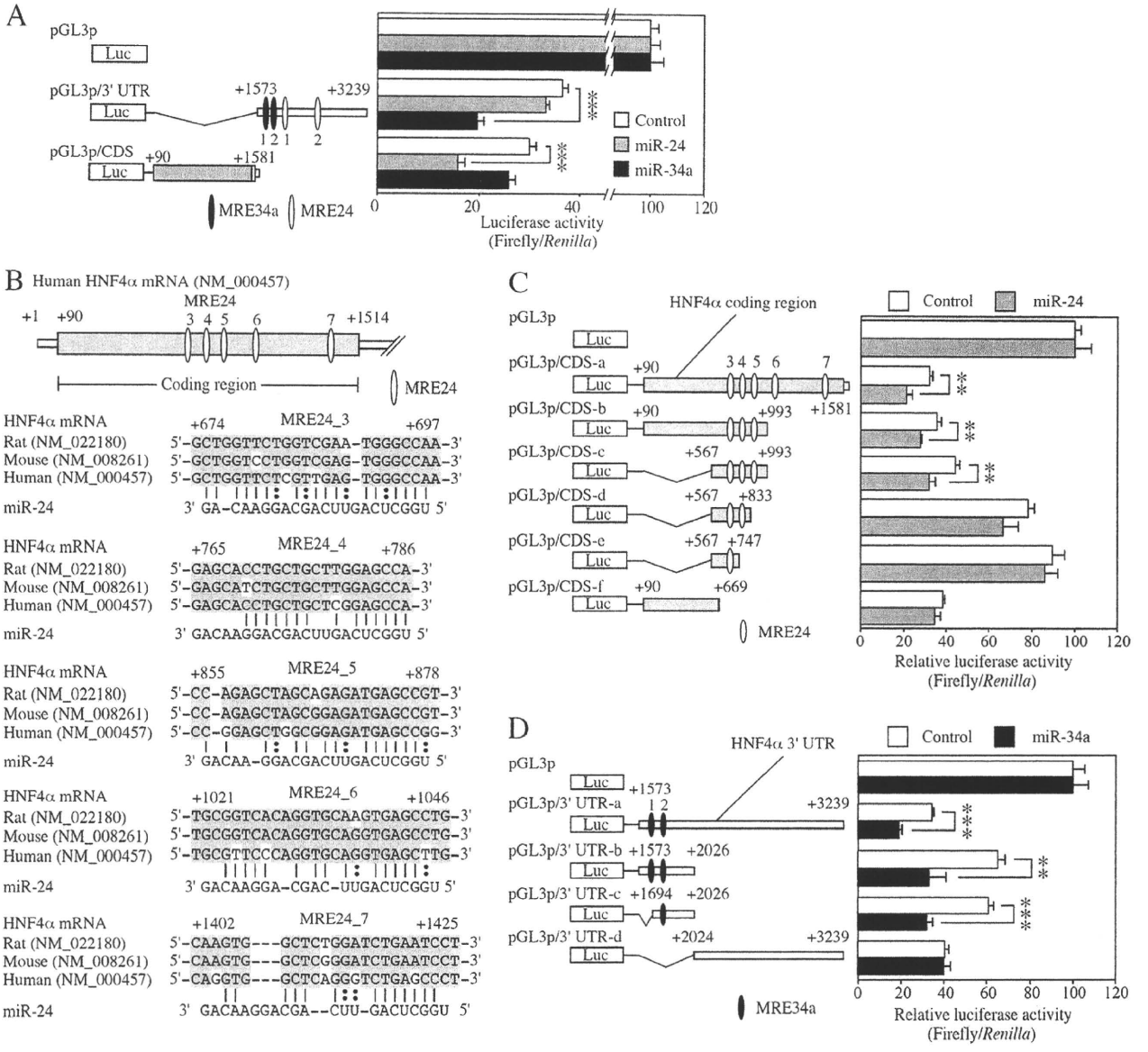

FIGURE 2. **Reporter analyses of MREs in the coding region and 3′-UTR of HNF4α mRNA.** *A*, reporter plasmids and pre-miR miRNA precursor molecules were co-transfected into HEK293 cells, and luciferase assays were performed after 48 h. The data were the firefly luciferase activities normalized with the *Renilla* luciferase activities relative to that of pGL3p co-transfected with each miRNA. Each column represents the mean ± S.D. of three independent experiments. ***, $p < 0.001$. *B*, schematic diagrams of the coding region of human HNF4α mRNA and mapping of predicted miR-24 target sites are described. Complementarity of miR-24 to the predicted target sequence of human HNF4α is also indicated. The conserved nucleotides are highlighted in *gray boxes*. *C* and *D*, luciferase assays were performed using plasmids containing MRE24 in the coding region (*C*) or MRE34a in the 3′-UTR (*D*) of HNF4α mRNA. The data were relative to that of pGL3p co-transfected with each miRNA. Each column represents the mean ± S.D. of three independent experiments. **, $p < 0.01$; ***, $p < 0.001$.

tides inserted in the coding region. When pre-miR miRNA precursor molecules for miR-24 and miR-34a were transfected into HepG2 cells, the mature miR-24 and miR-34a levels were increased 10.6- and 6.1-fold, respectively (data not shown). Concomitantly, the HNF4α protein levels were dramatically decreased. To investigate whether the decrease of the HNF4α protein levels was accompanied by a decrease of the mRNA levels, we determined the HNF4α mRNA levels by real time RT-PCR analysis. As shown in Fig. 1*C*, the HNF4α mRNA level was significantly decreased with the overexpression of miR-24, but not with miR-34a. These results suggested that miR-24 and miR-34a down-regulate the HNF4α expression by different mechanisms, *i.e.* mRNA degradation and translational repression, respectively.

Identification of Functional MRE in Coding Region and 3′-UTR of HNF4α mRNA—In the 3′-UTR of the HNF4α mRNA, two potential miRNA recognition elements for miR-24 (MRE24_1 and MRE24_2) and miR-34a (MRE34a_1 and MRE34a_2) were predicted (Fig. 1*A*). To investigate whether these MRE are functional in the down-regulation of the HNF4α, luciferase assays were performed using the pGL3p/3′-UTR plasmid containing 3′-UTR of HNF4α with HEK293 cells (Fig. 2*A*). The luciferase activity was significantly decreased by the overexpression of miR-34a, but not by miR-24. We next

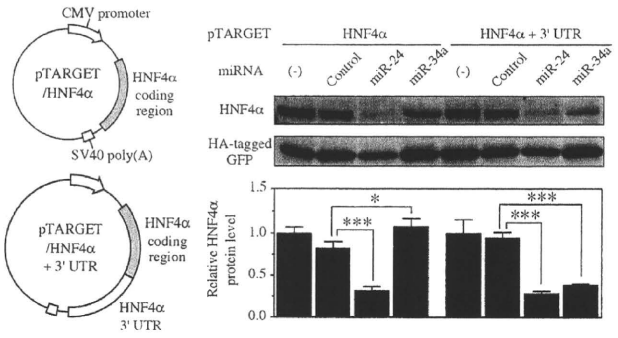

FIGURE 3. **Effects of miRNAs on the exogenous HNF4α expression in HEK293 cells.** The HNF4α expression plasmids including and excluding 3′-UTR used in this study are shown. These plasmids were transfected with HA-tagged GFP expression plasmid and pre-miR miRNA precursor molecules into HEK293 cells. After 48 h, whole cell lysates were prepared. The exogenously expressed HNF4α and HA-tagged GFP protein levels were determined by Western blot analyses. The data represent HNF4α protein level normalized with HA-tagged GFP level relative to that of no transfection (−). Each column represents the mean ± S.D. of three independent experiments. *, $p < 0.05$; ***, $p < 0.001$.

performed luciferase assays using the pGL3p/coding sequence (CDS) plasmid containing the coding region of HNF4α to examine the possibility that down-regulation of HNF4α by miR-24 might be mediated by elements in the coding region. The luciferase activity was significantly decreased by the overexpression of miR-24, although miR-34a did not affect the activity (Fig. 2*A*). These results prompted us to search for the potential recognition element of miR-24 in the coding region of HNF4α mRNA. Computational search using RNA22 identified five potential MRE24s (termed MRE24_3 to MRE24_7) in the coding region of HNF4α mRNA (Fig. 2*B*).

To identify the functional MREs, we performed luciferase assay using a series of deleted reporter constructs. Overexpression of miR-24 significantly decreased the luciferase activities of reporter constructs pGL3/CDS-b and pGL3/CDS-c containing MRE24_3 to _5 but did not affect the activity of the pGL3/CDS-f (Fig. 2*C*), indicating that three MREs would be functional. The deletion of MRE24_4 and 5 (pGL3p/CDS-d and -e) resulted in the loss of repression, suggesting that MRE24_3, 4, and 5 function cooperatively. Overexpression of miR-34a significantly decreased the activity of reporter constructs pGL3/3′-UTR-b containing MRE34a_1 and 2 but did not affect the activity of the pGL3/3′-UTR-d (Fig. 2*D*). The deletion of MRE34a_1 did not affect the repressive effects (pGL3p/3′-UTR-c), indicating that MRE34a_2 plays a key role in the miR-34a-mediated repression. Collectively, MRE24s in the coding region and MRE34a in the 3′-UTR of HNF4α mRNA would be functional.

miR-24 and miR-34a Act on the Coding Region and the 3′-UTR of HNF4α, Respectively—To verify that miR-24 and miR-34a act on the coding region and the 3′-UTR of HNF4α, respectively, we constructed expression systems of HNF4α that excluded or included the 3′-UTR. In the HEK293 cells transfected with pTARGET/HNF4α plasmid, the HNF4α protein level was significantly decreased by the overexpression of miR-24, but not by miR-34a (Fig. 3). In the HEK293 cells transfected with pTARGET/HNF4α+3′-UTR plasmid, the HNF4α protein level was significantly decreased by both miR-24 and miR-34a. These results support that miR-24 and miR-34a down-regulate the HNF4α expression through recognizing the elements in the coding region and the 3′-UTR of HNF4α mRNA, respectively.

Regulation of miR-24 and miR-34a Expression—The mature miR-24 is produced from two precursors, pre-miR-24-1 and pre-miR-24-2, the genes of which are located on chromosome 9q22.32 and 19p13.12, respectively. The mature miR-34a is produced from a precursor pre-miR-34a, the gene of which is located on chromosome 1p36.22. Because the HNF4α expression and/or activity are changed in response to signals derived from bile acids, we examined whether bile acids affect the expression of miR-24 and miR-34a. First, we examined the effect of chenodeoxycholic acid on the expression of the precursors of miR-24 and miR-34a. We found that the treatment with chenodeoxycholic acid increased the pre-miR-24-2 level in HepG2 cells (3.4-fold) at a concentration of 200 μM (data not shown). Bile acids are known to activate protein kinase C (PKC) and reactive oxygen species (ROS) generation. We next investigated the effects of PKC activator PMA and ROS generator H_2O_2 on the expression of the precursors of miR-24 and miR-34a. The treatment with PMA for 0.5–3 h markedly increased the expression of the pre-miR-24-2 level (Fig. 4*A*). The treatment with H_2O_2 for a relatively longer time greatly increased the expression levels of pre-miR-24-2 and pre-miR-34a (Fig. 4*B*). This was accompanied by increases of the mature miR-24 and miR-34a levels (Fig. 4*C*). Interestingly, the HNF4α protein levels were significantly decreased (Fig. 4*D*). It was considered that PMA or H_2O_2 repressed the HNF4α expression though increasing the miR-24 and miR-34a levels.

PKC activates MAPK pathway including ERK, JNK, and p38. The PMA-dependent induction of pre-miR-24-2 was decreased by co-treatment with MAPK/ERK kinase (MEK) inhibitor U0126 or p38 inhibitor SB202190 but not with JNK inhibitor SP600125 (Fig. 4*E*). In contrast, these MAPK inhibitors did not affect the H_2O_2-dependent induction of pre-miR-34a (Fig. 4*F*). These results suggest that the ERK and p38 MAPK pathways modulate the pre-miR-24-2 level. The decrease of the HNF4α expression via activation of MAPK or generation of ROS might partly be explained by the induction of miRNAs repressing HNF4α.

miR-24- and miR-34a-dependent Down-regulation of HNF4α Decreases the Expression of Target Genes—We next investigated the effects of the miRNA-dependent down-regulation of HNF4α on the expression of target genes (Fig. 5*A*). The overexpression of miR-24 and miR-34a drastically decreased the CYP7A1 mRNA level in HepG2 cells. In addition, the overexpression of miR-24 and miR-34a significantly decreased the CYP8B1, CYP27A1, and PEPCK mRNA levels. To investigate whether the decrease of these mRNAs resulted from the decrease of the HNF4α protein level but not the direct effects of miRNAs, we introduced siHNF4α into the HepG2 cells. It was clearly demonstrated that the HNF4α protein level was remarkably decreased by the transfection of siHNF4α (Fig. 5*B*). Under this condition, the mRNA levels of CYP7A1, CYP8B1, CYP27A1, and PEPCK were significantly decreased. These results suggest that the decrease of HNF4α by miR-24 and miR-34a caused the decrease of the expression of the target genes. Because they are key enzymes for the bile acid biosynthetic

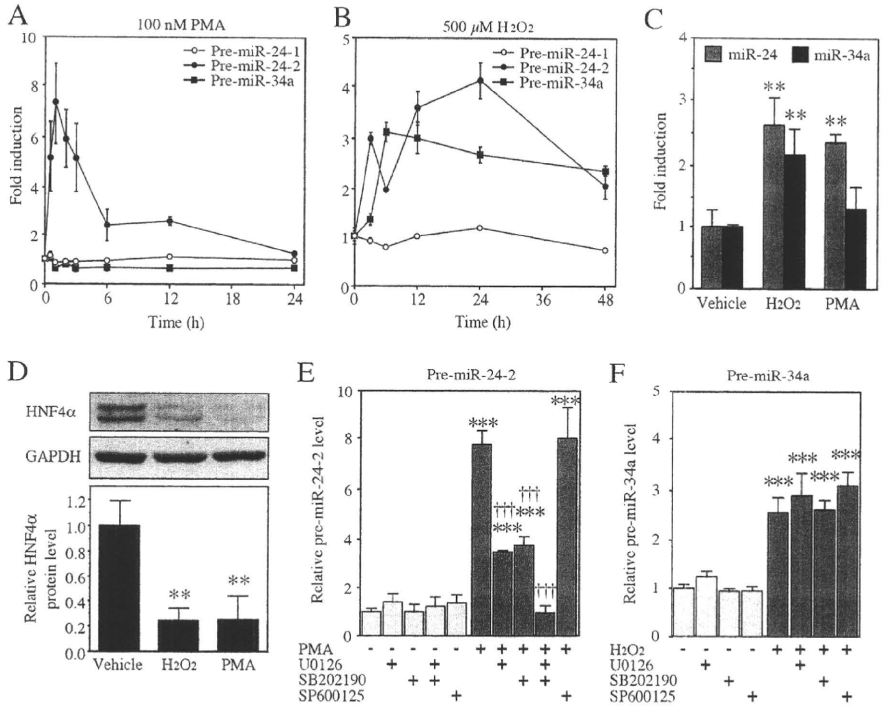

FIGURE 4. **Regulation of miR-24 and miR-34a through MAPK and ROS pathway, respectively.** *A* and *B*, HepG2 cells were treated with 100 nM PMA (*A*) or 500 μM H_2O_2 (*B*) for the indicated time. The pre-miRNA levels were determined by real time RT-PCR and normalized with the U6 small nuclear RNA level. The data are shown as fold changes compared with vehicle. Each point represents the mean ± S.D. of three independent experiments. *C* and *D*, HepG2 cells were treated with 100 nM PMA or 500 μM H_2O_2 for 48 h. The mature miR-24 and miR-34a levels were determined by real time RT-PCR and normalized with the U6 small nuclear RNA level (*C*). The HNF4α and GAPDH protein levels were determined by Western blot analyses (*D*). The data are relative to vehicle. Each column represents the mean ± S.D. of three independent experiments. **, $p < 0.01$, compared with vehicle. *E* and *F*, cells were co-treated with 100 nM PMA and 10 μM MAPK inhibitors for 1 h (*E*) or co-treated with 500 μM H_2O_2 and 10 μM MAPK inhibitors for 6 h (*F*). Each column represents the mean ± S.D. of three independent experiments. ***, $p < 0.001$, compared with nontreatment; †††, $p < 0.001$, compared with PMA-treated.

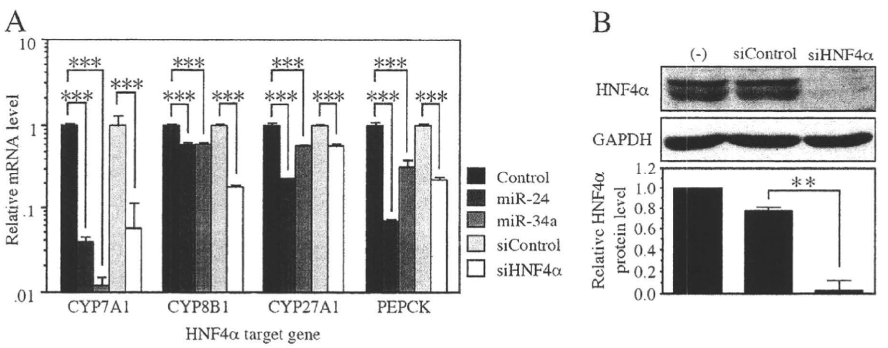

FIGURE 5. **Down-regulation of various HNF4α target genes by miR-24 and miR-34a as well as siHNF4α.** *A*, the mRNA levels of various targets of HNF4α in HepG2 cells were examined by real time RT-PCR and normalized with the GAPDH mRNA level. The data are relative to that transfected with control or siControl. Each column represents the mean ± S.D. of three independent experiments. ***, $p < 0.001$. *B*, the HNF4α and GAPDH protein levels in HepG2 cells were determined by Western blot analyses. The data are relative to no transfection (−). Each column represents the mean ± S.D. of three independent experiments. **, $p < 0.01$.

pathway and rate-limiting for gluconeogenesis, miR-24 and miR-34a may affect the hepatic functions through the regulation of HNF4α.

miR-24- and miR-34a-dependent Down-regulation of HNF4α Is Associated with Changes of Morphology and Cell Cycle Population—When miR-24 and miR-34a were overexpressed in the HepG2 cells, we noticed morphological changes including scattering and enlargement of the cells (Fig. 6*A*). Such morphological changes were also observed when the siHNF4α was transfected. It has been reported that HNF4α is involved in the control of differentiation, cell adhesion, and cell proliferation (15–17). We investigated the effects of overexpression of miR-24 and miR-34a on the cell cycle. The percentage of S phase cells was significantly decreased by the transfection with miR-24 or miR-34a into the HepG2 cells (Fig. 6*B*). The decrease was also observed by the transfection of siHNF4α. In addition, it was found that the transfection with miR-24 or miR-34a significantly induced the mRNA level of cyclin-dependent kinase inhibitor p21 (Fig. 6*C*), although there was no clear induction of p16 and p27. The induction of p21 and p16 was also observed when the siHNF4α was transfected. These results suggest that the changes of morphology and cell population by miR-24 and miR-34a might partly be due to the down-regulation of HNF4α. However, the transfection of siHNF4α did not cause cell cycle arrest at the G_1/S transition, although the overexpression of miR-24 and miR-34a caused complete arrest at the G_1/S transition, when the cells were synchronized by serum starvation (Fig. 6*D*). Thus, miR-24 and miR-34a may arrest the cell cycle through other mechanisms that are independent of HNF4α.

DISCUSSION

HNF4α is highly expressed in liver, although it is also expressed in extrahepatic tissues such as kidney, intestine, and pancreas (1). It is constitutively active and generally acts as a positive transcriptional regulator of the expression of various transcriptional factors and enzymes. It has been reported that knock-out of HNF4α disrupts the hepatic architecture and function (15). Mutations in HNF4α are a cause of type 1 maturity onset diabetes of the young, which is the monogenic form of diabetes that results from functional defects in islet β cells (18). Thus, HNF4α is critical for tissue development and for the maintenance of a number of metabolic pathways. In this study, we investigated the role of miRNAs in the regulation of HNF4α expression.

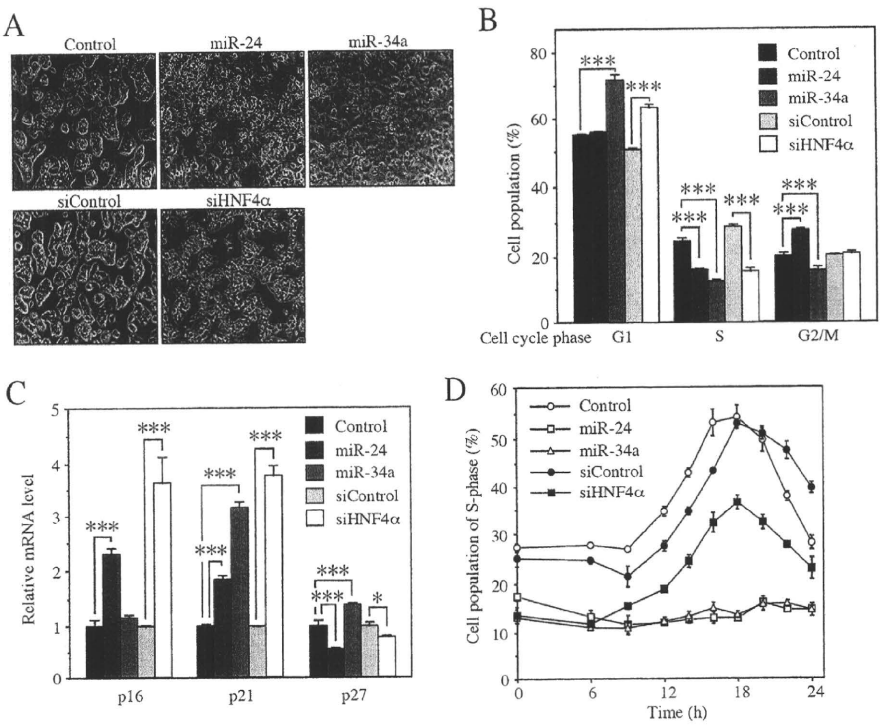

FIGURE 6. **Inhibition of G_1/S transition by miR-24 and miR-34a in HepG2 cells.** *A*, morphological change of HepG2 cells at 72 h after the transfection with pre-miRNA precursor molecules or siRNAs was visualized and photographed under a light microscope. *B*, cells were collected at 48 h after the transfection, and the cell population in each phase of cell cycle was analyzed by FACS. Each column represents the mean ± S.D. of three independent experiments. ***, $p < 0.001$. *C*, the p16, p21, and p27 mRNA levels were determined by real time RT-PCR and were normalized with the GAPDH mRNA level. The data are relative to that transfected with the control or siControl. Each column represents the mean ± S.D. of three independent experiments. *, $p < 0.05$; ***, $p < 0.001$. *D*, the time-dependent change of the percentages of cell population under S phase are shown. Twenty-four hours after the transfection with pre-miRNA precursor molecules or siRNAs, the cells were synchronized by serum deprivation for 24 h. Then the cells were restimulated with serum for the indicated time. Each point represents the mean ± S.D. of three independent experiments.

We found that both miR-24 and miR-34a negatively regulate the HNF4α expression. Generally, in vertebrates, miRNAs are believed to recognize elements in the 3′-UTR to repress the translation or to degrade mRNA. In this study, however, we found that the functional MREs for miR-24-dependent regulation are located in the coding region of HNF4α mRNA. This was not surprising because for other targets, it has been demonstrated the miRNA regulates through the coding region or 5′-UTR (19–21). miR-24 decreased the HNF4α mRNA level in addition to the protein level, suggesting that miR-24 is likely to repress the HNF4α expression through mRNA degradation rather than through translational repression. On the other hand, the functional MRE for miR-34a-dependent regulation is located in the 3′-UTR. miR-34a is likely to repress the HNF4α expression through translational repression, because it did not decrease the mRNA levels, although it did decrease the HNF4α protein level. Thus, it was considered that miR-24 and miR-34a regulate the human HNF4α expression through different mechanisms.

We found that the pre-miR-24-2 level was strongly increased by the treatment with PKC/MAPK activator PMA and ROS generator H_2O_2 in HepG2 cells. The activation of the PKC pathway induces cholestasis (22). The ROS pathway plays an important role in the pathogenesis of nonalcoholic steatohepatitis (23). Because the increase of the pre-miR-24-2 resulted in the increase of the mature miR-24 level, the mature miR-24 expression seems to be induced in these pathological conditions. Additionally, it has been reported that transforming growth factor-β, which is associated with fibrosis, increased the miR-24 level (24). Regarding HNF4α, it has been reported that cholestasis, hepatic steatosis, and fibrosis down-regulate the expression (25–27). Thus, the down-regulation of HNF4α in these diseases might be due to the induction of miR-24.

Previous studies revealed that miR-34a is regulated by p53, a tumor suppressor gene (28, 29). The present study demonstrated that the pre-miR-34a level was increased by the treatment with H_2O_2. The treatment with MAPK inhibitors failed to inhibit the induction of pre-miR-34a. ROS is known to activate p53 pathway, suggesting that the increase of pre-miR-34a might result from the p53 activation, but not MAPK pathways. It is known that chenodeoxycholic acid activates the PKC pathway and generates ROS, but it failed to increase the pre-miR-34a level in our study (data not shown). Although the reason for the discrepancy is unknown, it is surmised that miR-34a may be up-regulated directly by bile acids.

We found that the changes of morphology and cell population by miR-24 and miR-34a might be partly due to the down-regulation of HNF4α. However, detailed examination of the cell population revealed that cell cycle arrest might be caused by additional roles for miR-24 and miR-34a with other targets besides HNF4α. In fact, miR-34a is known to suppress cell cycle regulatory genes such as cyclin E2 and cyclin-dependent kinase 4, resulting in cell cycle arrest in the G_1 phase (30). Meanwhile, miR-24 has been reported to promote the proliferation of transforming growth factor-β-treated HuH7 hepatocellular carcinoma cells (24) as well as A549 lung carcinoma cells (31). These findings might be consistent with a report showing that miR-24 suppressed the translation of p16, which arrests cells in the G_1 phase (32). In contrast, Cheng *et al.* (31) have reported that miR-24 attenuated the proliferation in HeLa cells. Thus, miR-24 might function differently in different cells. In contrast to a previous study (33), the decrease of HNF4α by the transfection with siHNF4α resulted in the up-regulation of p21 gene expression. Because c-Myc interacts with HNF4α and blocks the activation of p21 promoter, the conflicting result might be due to the difference in the balance between c-Myc and HNF4α expression. Taken together, miR-24 and miR-34a would cause

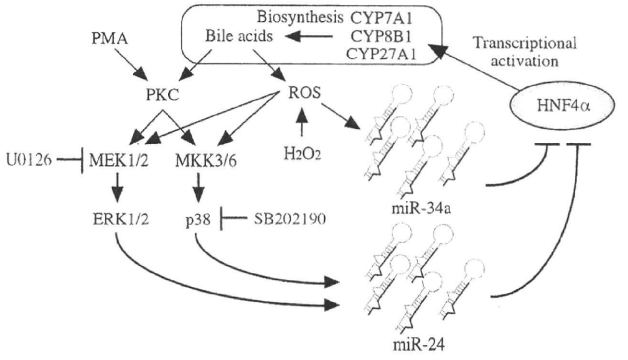

FIGURE 7. **A proposal of the regulatory loop of miR-24, miR-34a, and HNF4α in bile acid synthesis.** Bile acids are known to activate PKC and ROS generation, resulting in the activation of MAPK pathway. The miR-24 and miR-34a expression are induced by MAPK-dependent and -independent pathways, respectively. In turn, miR-24 and miR-34a negatively regulate the HNF4α. The down-regulation of HNF4α decreases the expression of bile acid-synthesizing enzymes CYP7A1 and CYP8B1, resulting in the decrease of bile acids.

cell arrest through the regulation of multiple targets in global network for cell cycle.

Of particular interest in our findings was that the miR-24- and miR-34a-dependent down-regulation of HNF4α resulted in decreases of the downstream genes. CYP7A1 catalyzes the first and rate-limiting step in the classical bile acid synthetic pathway (34). It is considered that the induction of miR-24 and miR-34a would result in decreased bile acid synthesis. In addition, gluconeogenic enzyme PEPCK was also down-regulated by the decrease of the HNF4α expression by miRNAs. Thus, miR-24 and miR-34a might affect the various hepatic functions through the negative regulation of HNF4α expression. Interestingly, we found that these miRNAs were induced by PKC/MAPK activator or ROS generator. Therefore, we propose a novel feedback regulation of bile acids synthesis (Fig. 7). Namely, bile acids activate PKC/MAPK and ROS pathways. The PKC/MAPK and ROS pathways increase the miR-24 and miR-34a expression, respectively. These miRNAs down-regulate the HNF4α expression. Accordingly, the expression of bile acid-synthesizing enzymes is decreased. Thus, we could provide new insight into the negative feedback regulation of bile acids synthesis.

In summary, we found that miR-24 and miR-34a regulate human HNF4α expression, resulting in the decrease of various downstream genes and aberrant cell cycle. Because these miRNAs are under the control of cellular stress, the miRNAs-dependent regulation of human HNF4α might contribute to pathology in liver.

Acknowledgment—We acknowledge Brent Bell for reviewing the manuscript.

REFERENCES

1. Gonzalez, F. J. (2008) *Drug Metab. Pharmacokinet.* **23,** 2–7
2. Kamiyama, Y., Matsubara, T., Yoshinari, K., Nagata, K., Kamimura, H., and Yamazoe, Y. (2007) *Drug Metab. Pharmacokinet.* **22,** 287–298
3. Hylemon, P. B., Zhou, H., Pandak, W. M., Ren, S., Gil, G., and Dent, P. (2009) *J. Lipid Res.* **50,** 1509–1520
4. Goodwin, B., Jones, S. A., Price, R. R., Watson, M. A., McKee, D. D., Moore, L. B., Galardi, C., Wilson, J. G., Lewis, M. C., Roth, M. E., Maloney, P. R., Willson, T. M., and Kliewer, S. A. (2000) *Mol. Cell* **6,** 517–526
5. Lee, Y. K., Dell, H., Dowhan, D. H., Hadzopoulou-Cladaras, M., and Moore, D. D. (2000) *Mol. Cell. Biol.* **20,** 187–195
6. Hatzis, P., Kyrmizi, I., and Talianidis, I. (2006) *Mol. Cell. Biol.* **26,** 7017–7029
7. Li, T., Jahan, A., and Chiang, J. Y. (2006) *Hepatology* **43,** 1202–1210
8. Guo, H., Gao, C., Mi, Z., Wai, P. Y., and Kuo, P. C. (2006) *Biochem. J.* **394,** 379–387
9. Popowski, K., Eloranta, J. J., Saborowski, M., Fried, M., Meier, P. J., and Kullak-Ublick, G. A. (2005) *Mol. Pharmacol.* **67,** 1629–1638
10. Bartel, D. P. (2004) *Cell* **116,** 281–297
11. Chang, J., Nicolas, E., Marks, D., Sander, C., Lerro, A., Buendia, M. A., Xu, C., Mason, W. S., Moloshok, T., Bort, R., Zaret, K. S., and Taylor, J. M. (2004) *RNA Biol.* **1,** 106–113
12. Krützfeldt, J., Rajewsky, N., Braich, R., Rajeev, K. G., Tuschl, T., Manoharan, M., and Stoffel, M. (2005) *Nature* **438,** 685–689
13. Hand, N. J., Master, Z. R., Le Lay, J., and Friedman, J. R. (2009) *Hepatology* **49,** 618–626
14. Sekine, S., Ogawa, R., Mcmanus, M. T., Kanai, Y., and Hebrok, M. (2009) *J. Pathol.* **219,** 365–372
15. Parviz, F., Matullo, C., Garrison, W. D., Savatski, L., Adamson, J. W., Ning, G., Kaestner, K. H., Rossi, J. M., Zaret, K. S., and Duncan, S. A. (2003) *Nat. Genet.* **34,** 292–296
16. Battle, M. A., Konopka, G., Parviz, F., Gaggl, A. L., Yang, C., Sladek, F. M., and Duncan, S. A. (2006) *Proc. Natl. Acad. Sci. U.S.A.* **103,** 8419–8424
17. Erdmann, S., Senkel, S., Arndt, T., Lucas, B., Lausen, J., Klein-Hitpass, L., Ryffel, G. U., and Thomas, H. (2007) *Biol. Chem.* **388,** 91–106
18. Stanger, B. Z. (2008) *Diabetes* **57,** 1461–1462
19. Forman, J. J., Legesse-Miller, A., and Coller, H. A. (2008) *Proc. Natl. Acad. Sci. U.S.A.* **105,** 14879–14884
20. Tay, Y., Zhang, J., Thomson, A. M., Lim, B., and Rigoutsos, I. (2008) *Nature* **455,** 1124–1128
21. Lytle, J. R., Yario, T. A., and Steitz, J. A. (2007) *Proc. Natl. Acad. Sci. U.S.A.* **104,** 9667–9672
22. Kubitz, R., Saha, N., Kühlkamp, T., Dutta, S., vom Dahl, S., Wettstein, M., and Häussinger, D. (2004) *J. Biol. Chem.* **279,** 10323–10330
23. Day, C. P. (2002) *Gut* **50,** 585–588
24. Huang, S., He, X., Ding, J., Liang, L., Zhao, Y., Zhang, Z., Yao, X., Pan, Z., Zhang, P., Li, J., Wan, D., and Gu, J. (2008) *Int. J. Cancer* **123,** 972–978
25. Geier, A., Zollner, G., Dietrich, C. G., Wagner, M., Fickert, P., Denk, H., van Rooijen, N., Matern, S., Gartung, C., and Trauner, M. (2005) *Hepatology* **41,** 470–477
26. Xie, X., Liao, H., Dang, H., Pang, W., Guan, Y., Wang, X., Shyy, J. Y., Zhu, Y., and Sladek, F. M. (2009) *Mol. Endocrinol.* **23,** 434–443
27. Yue, H. Y., Yin, C., Hou, J. L., Zeng, X., Chen, Y. X., Zhong, W., Hu, P. F., Deng, X., Zhang, J. P., Ning, B. F., Shi, J., Zhang, X., Lin, Y., and Xie, W. F. (2009) *Gut,* in press
28. Raver-Shapira, N., Marciano, E., Meiri, E., Spector, Y., Rosenfeld, N., Moskovits, N., Bentwich, Z., and Oren, M. (2007) *Mol. Cell* **26,** 731–743
29. Chang, T. C., Wentzel, E. A., Kent, O. A., Ramachandran, K., Mullendore, M., Lee, K. H., Feldmann, G., Yamakuchi, M., Ferlito, M., Lowenstein, C. J., Arking, D. E., Beer, M. A., Maitra, A., and Mendell, J. T. (2007) *Mol. Cell* **26,** 745–752
30. He, L., He, X., Lim, L. P., de Stanchina, E., Xuan, Z., Liang, Y., Xue, W., Zender, L., Magnus, J., Ridzon, D., Jackson, A. L., Linsley, P. S., Chen, C., Lowe, S. W., Cleary, M. A., and Hannon, G. J. (2007) *Nature* **447,** 1130–1134
31. Cheng, A. M., Byrom, M. W., Shelton, J., and Ford, L. P. (2005) *Nucleic Acids Res.* **33,** 1290–1297
32. Lal, A., Kim, H. H., Abdelmohsen, K., Kuwano, Y., Pullmann, R., Jr., Srikantan, S., Subrahmanyam, R., Martindale, J. L., Yang, X., Ahmed, F., Navarro, F., Dykxhoorn, D., Lieberman, J., and Gorospe, M. (2008) *PLoS One* **3,** e1864
33. Hwang-Verslues, W. W., and Sladek, F. M. (2008) *Mol. Endocrinol.* **22,** 78–90
34. Pikuleva, I. A. (2006) *Pharmacol. Ther.* **112,** 761–773